Order-by-disorder near criticality in XY pyrochlore magnets

Behnam Javanparast,[1] Alexandre G. R. Day,[1] Zhihao Hao,[1] and Michel J. P. Gingras[1,2,3]
[1]*Department of Physics and Astronomy, University of Waterloo, Waterloo, ON, N2L 3G1, Canada*
[2]*Canadian Institute for Advanced Research, 180 Dundas St. W., Toronto, ON, M5G 1Z8, Canada*
[3]*Perimeter Institute for Theoretical Physics, 31 Caroline St. N., Waterloo, ON, N2L 2Y5, Canada*
(Received 27 October 2014; revised manuscript received 23 April 2015; published 20 May 2015)

We consider a system of spins on the sites of a three-dimensional pyrochlore lattice of corner-sharing tetrahedra interacting with a predominant effective xy exchange. In particular, we investigate the selection of a long-range ordered state with broken discrete symmetry induced by thermal fluctuations near the critical region. At the standard mean-field theory (s-MFT) level, in a region of the parameter space of this Hamiltonian that we refer to as Γ_5 *region*, the ordered state possesses an accidental U(1) degeneracy. In this paper, we show that fluctuations beyond s-MFT lift this degeneracy by selecting one of two states (so-called ψ_2 and ψ_3) from the degenerate manifold, thus exposing a certain form of order-by-disorder (ObD). We analytically explore this selection at the microscopic level and close to criticality by elaborating upon and using an extension of the so-called TAP method, originally developed by Thouless, Anderson, and Palmer to study the effect of fluctuations in spin glasses. We also use a single-tetrahedron cluster-mean-field theory (c-MFT) to explore over what minimal length scale fluctuations can lift the degeneracy. We find the phase diagrams obtained by these two methods to be somewhat different since c-MFT only includes the shortest-range fluctuations. General symmetry arguments used to construct a Ginzburg-Landau theory to lowest order in the order parameters predict that a weak magnetic moment m_z along the local $\langle 111\rangle$ ($\hat{z}$) direction is generically induced for a system ordering into a ψ_2 state, but not so for ψ_3 ordering. Both E-TAP and c-MFT calculations confirm this weak fluctuation-induced m_z moment. Using a Ginzburg-Landau theory, we discuss the phenomenology of multiple phase transitions below the paramagnetic phase transition and within the Γ_5 long-range ordered phase.

DOI: 10.1103/PhysRevB.91.174424 PACS number(s): 75.10.−b, 75.10.Hk, 05.70.Fh

I. INTRODUCTION

In the study of condensed matter systems, mean-field theory [1] is often the simplest starting point to obtain a qualitative understanding of the essential physics at play prior to carrying out a more sophisticated analysis. A standard mean-field theory (s-MFT) replaces the many-body problem with a simpler problem of a one-body system interacting with an averaged field produced by the rest of the interacting particles. In systems with competing or frustrated interactions, s-MFT may yield a number of states with a degenerate minimum free energy below the mean-field critical temperature, $T_c^{\rm MF}$ [2,3]. If these degeneracies are accidental, that is not imposed by exact symmetries of the Hamiltonian, they may be lifted by the effects of thermal [4] or quantum [5] fluctuations, a phenomenon known as order-by-disorder (ObD) [4–8].

The concept of ObD was originally proposed by Villain and collaborators as the ordered state selection mechanism for a two-dimensional frustrated Ising model on the domino lattice [4]. Since this seminal work, ObD has been theoretically identified and discussed for many highly frustrated magnetic models [6–18]. These systems generically possess an exponentially [$\exp(N^\alpha)$] large number of classical ground states (here N is the number of spins in the system and $\alpha \leqslant 1$). As a result, highly frustrated magnetic systems are intrinsically very sensitive to fluctuations or energetic perturbations. In the context of experimental studies of real materials, it is difficult to distinguish a selection of an ordered state via fluctuations from one that would arise from energetic perturbations beyond the set of interactions considered in a restricted theoretical model. Consequently, undisputed examples of ObD in experiments have remained scarce [19–21].

Quite recently, following an original proposal going back ten years [22,23], and building on an earlier study [24], several papers [15–18] have put forward compelling arguments for ObD being responsible for the experimentally observed long-range order in the insulating rare-earth pyrochlore oxide [25] $Er_2Ti_2O_7$. In this compound, Er^{3+} is magnetic and Ti^{4+} is not. The key observation in those works is that the accidentally degenerate classical ground states are related by operations with a U(1) symmetry [16]. This set of classically degenerate states form the so-called Γ_5 *manifold* [26]. For a range of interaction parameters of the most general symmetry-allowed bilinear nearest-neighbor pseudospin 1/2 exchange-like Hamiltonian [referred to as $\mathcal{H}$ in Eq. (1a) below] on the pyrochlore lattice of corner-sharing tetrahedra (see Fig. 3), the U(1) degeneracy is exact at the s-MFT level as long as the cubic symmetry of the system remains intact. As a shorthand, we henceforth refer to this region of exchange parameter space as the Γ_5 *region*, as referred to in the Abstract. Reference [16] showed that the U(1) symmetry is robust against a wide variety of perturbations added to $\mathcal{H}$ and argued that essentially only fluctuations can efficiently lift the degeneracy in $Er_2Ti_2O_7$ when considering bilinear anisotropic interactions of arbitrary range between the pseudospins.[1] Similar arguments were made in Ref. [15]. In this compound, a particular long-range ordered state, the ψ_2 state (see Fig. 1) [22,23,26–30], is selected.

[1]It has been pointed out by McClarty *et al.* that the ψ_2 state can be energetically selected through a van Vleck-like mechanism [43]. Reference [16] argues that this mechanism is too weak by several orders of magnitude to be at play in $Er_2Ti_2O_7$. However, a recent paper [30] questions this assertion.

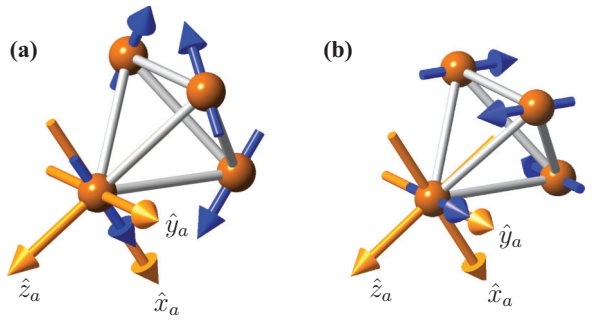

FIG. 1. (Color online) Spin configurations of the (a) noncoplanar ψ_2 state, as observed in $Er_2Ti_2O_7$ [26], and the (b) coplanar ψ_3 state on a single tetrahedron. The pattern is the same on all tetrahedra in a pyrochlore lattice which is a face-centered cubic lattice with a tetrahedron basis and these two states, which belong to the Γ_5 manifold, are thus said to have a $\boldsymbol{k} = 0$ ordering wave vector. The spin (in blue) at the a sublattice points along (a) the $\hat{x}_a$ axis of the local [111] reference frame for the ψ_2 state and along (b) the $\hat{y}_a$ axis of the same local frame for the ψ_3 state. The local $\hat{z}_a$ axis at sublattice a points along the local cubic [111] axis at that site such that the local $\hat{x}_a$, $\hat{y}_a$, $\hat{z}_a$ triad of orthogonal unit vectors (orange arrows) fulfills $\hat{x}_a \times \hat{y}_a = \hat{z}_a$. As illustrated in panels (a) and (b), the local $\hat{z}_a$ axis for sublattice a points directly out of the tetrahedron primitive basis cell. See Appendix A for more details.

Considering $\mathcal{H}$ on the pyrochlore lattice, Wong *et al.* [17] and Yan *et al.* [31] studied the effect of quantum [17,31] and thermal [31] fluctuations and established a general phase diagram for this Hamiltonian at $T = 0^+$.

The investigations reported in Refs. [14–17,31] focused on identifying the mechanism of *ground state* selection by taking into account the harmonic quantum [14–17,31] or classical [14,31] spin fluctuations about a classical long-range ordered state. On the other hand, the problem of state selection at temperatures near the critical transition temperature to the paramagnetic phase has received significantly less attention. Although there have been numerical studies of ObD selection of the ψ_2 state at $T \lesssim T_c$ [14,15,22,23,31–33], or upon approaching T_c from above [18], an analytical study specifying the role of the individual microscopic anisotropic spin-spin interactions in the ObD mechanism at $T \approx T_c$ has, to the best of our knowledge, not yet been carried out. The problem of selection at $T \lesssim T_c$ is not only of relevance to the phenomenology of $Er_2Ti_2O_7$ or other pyrochlore magnetic compounds [25], but it is of considerable interest for all highly frustrated magnetic systems proposed to display an ObD mechanism.

There are situations where a sort of ObD occurs near T_c which differ from the textbook cases [4–6,8] where the state selection near $T = 0^+$, proceeding either via thermal or quantum selection, is leveraged upon all the way to the long-range ordered state selected at T_c. For example, the long-range ordered state selected by ObD can in principle be different for the $T = 0^+$ and $T \lesssim T_c$ regimes. This occurs, for example, for classical Heisenberg spins on the pyrochlore lattice interacting via nearest-neighbor antiferromagnetic exchange and indirect Dzyaloshinskii-Moriya interaction [33,34]. In another class of problems, different competing long-range ordered states may have the same free energy at the s-MFT level only over a finite temperature interval, $T^* \leqslant T \leqslant T_c$ with a transition to a *nondegenerate* classical ground state at T^*. There, thermal fluctuation corrections to s-MFT can select one of the competing states over the $T^* \leqslant T \leqslant T_c$ window. This is what is predicted to occur in the multiple-$\boldsymbol{k}$ state selection in the $Gd_2Ti_2O_7$ pyrochlore antiferromagnetic between 0.7 and 1.0 K [35]. Perhaps the most exotic cases arise when a relic of ObD occurs at the critical temperature, while the classical ground state is *not* degenerate for the Hamiltonian considered, but would be for a closely related Hamiltonian minus some degeneracy-lifting weak energetic perturbations [14,36,37]. At the phenomenological Ginzburg-Landau level description, these cases are not paradoxical. They only become so when one is trying to ascribe a microscopic description to the physics at stake and the origin for, at least, one further equilibrium thermodynamic phase transition at some temperature below the paramagnetic transition at T_c. Finally, and generally speaking, one may ask whether a discussion of ObD at $T = 0^+$ is of pragmatic usefulness given that most experiments for which ObD may pertain typically proceed by cooling a material from a paramagnetic disordered phase to an ordered phase and not going below a certain baseline nonzero temperature constrained by the experimental setup. This broader context provides the motivation for our work which aims to go beyond the sole consideration of a phenomenological Ginzburg-Landau theory that contains all terms, relevant or not (in the renormalization-group sense), allowed by symmetry and to expose how the different competing microscopic interactions participate to the degeneracy-lifting near the transition at T_c.

In the temperature regime near a phase transition, the harmonic approximation describing low-energy excitations usually employed in theoretical discussions of ObD [5–8] at $T = 0^+$ is not physically justified since large fluctuations typically accompany the phase transition to the paramagnetic state. From a fundamental viewpoint, it is thus highly desirable to study the role of fluctuations beyond s-MFT using a different method that can be applied at temperatures close to the critical region. A possible route to tackle this problem was paved by Thouless, Anderson, and Palmer (TAP) in their study of the effect of fluctuations in spin glasses [38]. For the case of the Ising spin glass model, Plefka showed that the TAP correction can be systematically derived using a perturbative expansion [39]; an approach that was later generalized by Georges and Yedidia who calculated higher-order terms in the Plefka's perturbative expansion [40]. This approach, which we refer to as extended TAP (E-TAP), consists of a high-temperature expansion in $\beta \equiv 1/k_B T$ about the s-MFT solution. It captures corrections to the s-MFT free energy by including fluctuations in the form of on-site linear and nonlinear susceptibilities. A second approach allowing one to go beyond s-MFT is the cluster mean-field theory (c-MFT) [41,42]. This approach treats short-range fluctuations within a finite cluster exactly while taking into account the intercluster interactions in a mean-field fashion.

In the present work, we focus on the problem of ObD selection near criticality in a spin model on the pyrochlore lattice with predominant xy interactions using the E-TAP method. We have recently used this method to investigate

the problem of partial multiple-$\boldsymbol{k}$ order in pyrochlore magnets [35]. In this paper, we also employ c-MFT. We concentrate on the Γ_5 manifold for the $T \lesssim T_c^{\rm MF}$ regime since Γ_5 is not only an interesting theoretical playground according to recent investigations [14–17,30–32,43], it is also of potential relevance to real pyrochlore materials, such as $Er_2Ti_2O_7$, proposed to display an ObD mechanism [15,16,22,29]. In addition, the interesting case of distinct ObD selection at $T = 0^+$ and T_c, reported in a pyrochlore system with anisotropic spin-spin coupling [33], further motivates us in investigating the role of the various spin interactions in the state selection at $T \lesssim T_c$ in a general model of interacting spins on the pyrochlore lattice.

The rest of the paper is organized as follows. In Sec. II, we present the bilinear nearest-neighbor spin model defined by the Hamiltonian $\mathcal{H}$ of Eq. (1a) on the pyrochlore lattice and discuss its symmetries. Focusing on the Γ_5 manifold, we present a Ginzburg-Landau (GL) symmetry analysis to specify the general form of the lowest-order anisotropic terms allowed in the GL free energy ($\mathcal{F}_{\rm GL}$) that can lift the accidental U(1) degeneracy found in s-MFT. We show that the fluctuation correction terms to the s-MFT free energy select either the ψ_2 or the ψ_3 long-range ordered state of the Γ_5 manifold (see Fig. 1 and Appendix A for definitions) as well as induce a weak moment m_z along the local [111] direction for the ψ_2 state. In Sec. III A, we present the E-TAP method and determine the phase boundary at T_c between the ψ_2 and ψ_3 states in the space of anisotropic spin-spin coupling constants. We investigate in Sec. III B how short-ranged fluctuations acting on the length-scale of a single-tetrahedron can lead to ObD when incorporated in the self-consistent scheme of c-MFT. The c-MFT method also allows us to explore semi-quantitatively the role of nonzero effective Ising exchange (J_{zz}) on the selection at T_c. In Sec. IV, we briefly discuss the possibility of multiple phase transitions in xy pyrochlore magnets as temperature, for example, is varied. Finally, we close with a discussion in Sec. V. A number of appendices are provided to assist the reader with the technical details of the E-TAP calculations. In Appendix A, we detail the spin configurations of the ψ_2 and ψ_3 states. In Appendix B, we analyze the symmetry properties of the ψ_2 and the ψ_3 states to show that a fluctuation-induced local m_z moment is only compatible with a ψ_2 long-range ordered state. We provide in Appendix C the details of the E-TAP calculations and the diagrammatic approach employed.

II. MODEL

We consider the following Hamiltonian on the pyrochlore lattice [16,44]:

$$\mathcal{H} = \mathcal{H}_0 + \mathcal{H}_1, \tag{1a}$$

$$\mathcal{H}_0 = \sum_{\langle ij \rangle} J_{zz} S_i^z S_j^z - J_\pm (S_i^+ S_j^- + S_i^- S_j^+), \tag{1b}$$

$$\mathcal{H}_1 = \sum_{\langle ij \rangle} J_{\pm\pm} (S_i^+ S_j^+ \gamma_{ij} + S_i^- S_j^- \gamma_{ij}^*) + J_{z\pm} \{ S_i^z (\zeta_{ij} S_j^+ + \zeta_{ij}^* S_j^-) + i \leftrightarrow j \}, \tag{1c}$$

where $S_i^\pm \equiv S_i^x \pm i S_i^y$ and S_i^μ, with $\mu = z, +, -$, is defined in the local [111] coordinate frame [44] attached to each of the four pyrochlore sublattices (see Fig. 1). $\boldsymbol{S}_i$ can be treated classically as a three-component vector or quantum mechanically as an operator such as a $\boldsymbol{S}_i = 1/2$ pseudospin. In the context of magnetic rare-earth pyrochlores, $\boldsymbol{S}_i$ would represent either the total angular momentum $\boldsymbol{J}$ within a simplified model of $\boldsymbol{J}$-$\boldsymbol{J}$ coupling [30,45–47], or a pseudospin 1/2 describing the single-ion ground state doublet [15,16,25,44–48].

As we are foremost interested in the selection of classical ordered phases at $0 \ll T \lesssim T_c$, we shall treat $\boldsymbol{S}_i$ generally classically with $|\boldsymbol{S}_i| = 1/2$ for all i. However, in Sec. III B, where we use the c-MFT method, we consider $\boldsymbol{S}_i = 1/2$ quantum mechanically, mostly for computational ease. In Eq. (1), J_{zz}, $J_\pm$, $J_{\pm\pm}$, and $J_{z\pm}$ are the four symmetry-allowed independent nearest-neighbor exchange parameters, while $\zeta_{ij} = -\gamma_{ij}^*$ are bond-dependent phases on a single tetrahedron defined in Refs. [16,44,48].[2]

It is important for the discussion that follows to split $\mathcal{H}$ into the two terms $\mathcal{H}_0$ and $\mathcal{H}_1$ in Eq. (1a) and consider the symmetry properties of each term. $\mathcal{H}_0$ has a U(1) symmetry: it is invariant under a rotation of $\boldsymbol{S}_i$ by an arbitrary global angle about the local $\langle 111 \rangle$ axes. On the other hand, the $\mathcal{H}_1$ term in Eq. (1a) is only invariant under rotations of $\boldsymbol{S}_i$ by $\frac{2\pi}{3}$, reducing the symmetry of $\mathcal{H}$ to Z_6 ($C_3[111] \times Z_2$).

We consider an s-MFT treatment of the Hamiltonian of Eq. (1), which orders in a state with a $\boldsymbol{k} = 0$ ordering wave vector in a certain region of the parameter space centered around a dominant $J_\pm$ (Γ_5 region). In this state, all the magnetic moments in the system lie predominantly perpendicular to the local [111] direction and point in the same direction in the local coordinate system (see Fig. 1). These spin configurations define the Γ_5 manifold [26]. As a result, $\boldsymbol{m}_i \equiv \langle \boldsymbol{S}_i \rangle$, the on-site magnetization,[3] and $\phi_i \equiv \tan^{-1}(m_i^y / m_i^x)$, the azimuthal angle expressed in the local [111] coordinate system, are independent of the lattice site index i. We henceforth drop the index i of ϕ_i and $\boldsymbol{m}_i$ for these $\boldsymbol{k} = 0$ spin configurations.

As first noted in Ref. [16], in the Γ_5 region, the s-MFT free energy is *independent* of ϕ and the system displays an accidental U(1) symmetry within such a s-MFT description. However, since $\mathcal{H}$ only has a global Z_6 symmetry, we expect that in a treatment of the problem that goes beyond s-MFT, this "artificial" U(1) symmetry to be reduced to a Z_6 symmetry in the paramagnetic phase, which gets spontaneously broken in the ordered phase. In this context, we note that a high-temperature series expansion of the quantum model (1a), with values $\{J_\pm, J_{\pm\pm}, J_{z\pm}, J_{zz}\}$ appropriate for $Er_2Ti_2O_7$ [16], shows explicitly that such a Z_6 anisotropy develops *in the paramagnetic phase* upon approaching T_c from above [18]. Also, a recent Monte Carlo study has investigated the critical behavior of a classical version of this model [32]. We now present a Ginzburg-Landau (GL) symmetry analysis that allows one to anticipate the form of the lowest order fluctuation corrections to s-MFT that lift the U(1) degeneracy.

[2] It has recently been pointed out by Y.-P. Huang, G. Chen, and M. Hermele [49] that there are cases (for example, Nd^{3+} in $Nd_2Zr_2O_7$ and Dy^{3+} in $Dy_2Ti_2O_7$) where the single-ion ground state doublet is a so-called "dipolar-octupolar" doublet in which γ_{ij} is *independent* of the $\langle i,j \rangle$ bond.

[3] $\langle \cdots \rangle$ represents a thermal Boltzmann average.

Ginzburg-Landau (GL) symmetry analysis

We start by defining the complex variable

$$m_{xy} \equiv \sqrt{m_x^2 + m_y^2}\exp(i\phi), \tag{2}$$

which corresponds to the magnitude and direction of the on-site magnetization $\boldsymbol{m} = \langle \boldsymbol{S}_i \rangle$ in the local xy plane.

For simplicity, we first consider a strictly local-xy state and assume $m_z = 0$. The allowed terms in the Ginzburg-Landau (GL) free energy can only be of even powers in m_{xy} due to time-reversal symmetry, τ. On the other hand, the rotation by $2\pi/3$ about the cubic $\langle 111 \rangle$ axes, or C_3 symmetry, forbids the existence of terms of the form $m_{xy}^n + (m_{xy}^*)^n$ unless n is a multiple of three. The resulting terms have the ability to lift the accidental U(1) degeneracy of the Γ_5 manifold since they introduce a dependence of the GL free energy on the azimuthal angle ϕ, the orientation of $\boldsymbol{m}$ in the local xy plane [see Eq. (2)]. Considering the effect of C_3 and τ together, assuming strictly xy order ($m_z = 0$), the lowest order term that breaks the U(1) symmetry must therefore have $n = 6$ and be of the form

$$\eta_6(T)\left[m_{xy}^6 + (m_{xy}^*)^6\right], \tag{3}$$

where the anisotropy strength η_6 depends on temperature T. We note that such a sixth order term is dangerously irrelevant for the three-dimensional xy universality class.[4] This means that while it does not affect the critical properties of the system [32,50], this term plays a crucial role in the selection of a specific long-range ordered state by lifting the U(1) s-MFT degeneracy at $T \lesssim T_c$. Higher-order terms $f_{6n} \sim |m_{xy}|^{6n}$ $(n > 1)$ are also generated by fluctuations, but are even more irrelevant than f_6 at T_c. As an example, we discuss in Sec. IV the effects of competing f_6 and f_{12} terms at $T < T_c$ as the amplitude $|m_{xy}|$ grows upon cooling below T_c.

If we now include the z component of the order parameter, i.e., $m_z \neq 0$, a U(1) symmetry-breaking term arises at fourth order in the components of $\boldsymbol{m}$ in the GL free energy. Such a term was only recently noted in a numerical study [30] but whose microscopic and symmetry origins were not discussed. Again, based on the combined effect of the C_3 and τ symmetry operations, the degeneracy-lifting fourth order term in the GL free energy has the form

$$\omega(T) m_z\left[m_{xy}^3 + (m_{xy}^*)^3\right], \tag{4}$$

where, here again, the anisotropic coupling ω depends on T. Together, Eqs. (3) and (4) identify the form of the two lowest-order terms in the GL free energy capable of lifting the degeneracy within the Γ_5 manifold.

It turns out that the sixth order term of Eq. (3) and the fourth order term of Eq. (4) have the same net effect in lifting the degeneracy beyond s-MFT as can be shown by combining them into a single term in the GL free energy, $\mathcal{F}_{\rm GL}$. Consider first the quadratic terms in $\mathcal{F}_{\rm GL}$ of the form $r_0(m_x^2 + m_y^2) + r_1 m_z^2$. Here r_0 and r_1 are chosen to be different to emphasize the distinct criticality for the xy and z components of the order parameter $\boldsymbol{m}$. Next, taking into account the terms of Eqs. (3) and (4), we have

$$\begin{aligned}\mathcal{F}_{\rm GL} = {} & r_0\left(m_x^2 + m_y^2\right) + r_1 m_z^2 + \omega m_z\left[m_{xy}^3 + (m_{xy}^*)^3\right] \\ & + \eta_6\left[m_{xy}^6 + (m_{xy}^*)^6\right] + \mathcal{F}_{\rm GL}^{(4)}(m_{xy}, m_z) \\ & + \mathcal{F}_{\rm GL}^{(6)}(m_{xy}, m_z) + \cdots .\end{aligned} \tag{5}$$

This can be rewritten as

$$\begin{aligned}\mathcal{F}_{\rm GL} = {} & r_0\left(m_x^2 + m_y^2\right) + r_1\left[m_z + \frac{\omega|m_{xy}|^3\cos(3\phi)}{r_1}\right]^2 \\ & - \frac{\omega^2|m_{xy}|^6}{2r_1} + \left(2\eta_6 - \frac{\omega^2}{2r_1}\right)|m_{xy}|^6\cos(6\phi) \\ & + \mathcal{F}_{\rm GL}^{(4)}(m_{xy}, m_z) + \mathcal{F}_{\rm GL}^{(6)}(m_{xy}, m_z) + \cdots ,\end{aligned} \tag{6}$$

where we used Eq. (2) to go from Eqs. (5) to (6). In Eqs. (5) and (6), $\mathcal{F}_{\rm GL}^{(4)}$ and $\mathcal{F}_{\rm GL}^{(6)}$ are fourth- and sixth-order terms and $\cdots$ represents terms that are of higher order in the components of $\boldsymbol{m}$. We take $r_1 > 0$ to enforce no criticality for the m_z component of $\boldsymbol{m}$. Upon minimizing Eq. (6) with respect to m_z, we obtain

$$m_z = -\omega|m_{xy}|^3\cos(3\phi)/r_1. \tag{7}$$

Hence, after having minimized $\mathcal{F}_{\rm GL}$ with respect to m_z, we have

$$\delta\mathcal{F}_{\rm GL}(\phi) \equiv 2\bar{\eta}_6|m_{xy}|^6\cos(6\phi), \tag{8}$$

with

$$2\bar{\eta}_6 \equiv (2\eta_6 - \omega^2/2r_1), \tag{9}$$

and where $\delta\mathcal{F}_{\rm GL}(\phi)$ is the anisotropic part of $\mathcal{F}_{\rm GL}$, the U(1) degeneracy-lifting term on which we focus. The minimum of $\delta\mathcal{F}_{\rm GL}$ is either $\cos(6\phi) = \pm 1$ depending on the sign of $\bar{\eta}_6$. This happens for $\phi = n\pi/3$ or $\phi = (2n+1)\pi/6$, with $n = 0, 1, \ldots, 5$ with these two sets of angles corresponding, respectively, to the ψ_2 and the ψ_3 states (see Fig. 1). So, when $\bar{\eta}_6 < 0$ ($\bar{\eta}_6 > 0$), the minimum free-energy state is ψ_2 (ψ_3). The boundary between ψ_2 and ψ_3 is thus determined by the real roots of $\bar{\eta}_6$. A similar discussion is invoked in Ref. [17] to describe the zero temperature ψ_2-ψ_3 phase boundaries arising from quantum ObD.

We note that the fluctuation corrections to s-MFT induce a local m_z moment to the minimum free-energy state, which was found to be strictly ordered in the local xy plane at the s-MFT level.[5] Since this moment is proportional to $\cos(3\phi)$, only the ψ_2 state can have a nonzero m_z. This result is also expected based solely on symmetry considerations for the ψ_2 and ψ_3 states (see Appendix B). The induced moment is, however, small just below T_c since it is proportional to $|m_{xy}|^3$ and inversely proportional to r_1 which remains firmly positive away from spontaneous Ising criticality at $r_1 = 0$.

[4] It is dangerously irrelevant since at temperatures $T < T_c$ this becomes relevant above a length scale λ, which diverges as a power of the correlation length [32,50].

[5] We note that, as we were concluding the present work, a very recent paper by Petit *et al.* [30] building on the model of Ref. [43], also reported a weak m_z moment in a mean-field theory calculation considering anisotropic $\boldsymbol{J}$-$\boldsymbol{J}$ couplings and the crystal electric field of $Er_2Ti_2O_7$.

At the phenomenological GL level, Eq. (8) is the final result demonstrating how the U(1) degeneracy at the s-MFT level may be lifted by the anisotropic terms of Eqs. (3) and (4). In this work, however, we are rather interested in exposing how the coefficient of the symmetry-breaking terms in the free energy of Eq. (6), $\bar{\eta}_6$, can be determined *at a microscopic level* when going beyond a s-MFT description. Specifically, we wish to explore the leading dependence of $\bar{\eta}_6$ upon the $J_{\pm\pm}$, $J_{z\pm}$, and J_{zz} anisotropic exchange couplings near T_c.

III. METHODS AND RESULTS

In Sec. III A, we use the E-TAP method to compute the phase boundary between the ψ_2 and ψ_3 states determined by the function $\bar{\eta}_6$ in Eq. (8) for $T \lesssim T_c^{\mathrm{MF}}$. In this calculation, we consider for simplicity $J_{zz} = 0$ in Eq. (1).[6] In Sec. III B, we conduct a complementary numerical study of fluctuation corrections to the s-MFT using cluster-MFT (c-MFT), which allows us to explore the effect of fluctuations at the level of one tetrahedron for both $J_{zz} = 0$ and $J_{zz} \neq 0$. Since we are essentially interested in the Γ_5 region where the dominant interaction is $J_\pm$ in Eq. (1), we express the rest of the couplings in units of $J_\pm$ and we henceforth denote the scaled (perturbative) interactions with lower case letters, i.e., $j_{\pm\pm} \equiv J_{\pm\pm}/J_\pm$ and $j_{z\pm} \equiv J_{z\pm}/J_\pm$.

A. Extended-TAP Method (E-TAP)

1. Method

In a magnetic system with static magnetic moments, a given moment is subject to a local field due to its neighbors. In an s-MFT treatment, the moment affects its own local field indirectly; this is an artifact of s-MFT. The so-called Onsager reaction field introduces a term in the s-MFT free energy that cancels this unphysical effect to leading order. As was shown by Thouless, Anderson, and Palmer (TAP) [38], this reaction-field correction is particularly important in setting up a proper mean-field theory description of spin glasses with infinite-range interactions [51]. Here, we present an extended version of the TAP method (E-TAP) first developed by Georges and Yedidia [40] for Ising spin glasses and which includes the lowest-order fluctuation corrections originally calculated by TAP as well as those beyond.

To proceed, we must first modify the E-TAP procedure of Ref. [40] to study the case of three-component classical spins with anisotropic exchange interactions. In the E-TAP method, nonzero on-site fluctuations, i.e., $\langle S_i^\alpha S_i^\beta \rangle \neq \langle S_i^\alpha \rangle \langle S_i^\beta \rangle$ [40], are taken into account via a high-temperature expansion (small β) of a Gibbs free energy:

$$G = -\frac{1}{\beta} \ln \mathrm{Tr} \left\{ \exp \left[-\beta \mathcal{H} + \sum_i \boldsymbol{\lambda}_i \cdot (\boldsymbol{S}_i - \boldsymbol{m}_i) \right] \right\}. \quad (10)$$

Here, $\boldsymbol{m}_i$ is the average magnetization at site i, $\boldsymbol{m}_i \equiv \langle \boldsymbol{S}_i \rangle$ and $\boldsymbol{\lambda}_i$ is a Lagrange multiplier, which fixes $\boldsymbol{m}_i$ to its mean-field value. The high-temperature expansion introduces fluctuations about the s-MFT solution. Defining $\beta G(\beta) \equiv \tilde{G}(\beta)$, the first two terms of the expansion in powers of β, $\tilde{G}(0)/\beta$ and $\tilde{G}'(0)$, are the entropy and energy at the s-MFT level, respectively. The prime represents differentiation with respect to β. The higher-order terms in the β expansion of the Gibbs free energy correspond to fluctuation corrections to the s-MFT free energy that generate the terms that lift the U(1) degeneracy. We aim to calculate the higher-order terms (beyond β^2) in the β expansion of Eq. (10) that contribute to the degeneracy lifting term $2\bar{\eta}_6 |m_{xy}|^6 \cos(6\phi)$ of Eq. (8) to lowest order in the coupling constants $j_{\pm\pm}$ and $j_{z\pm}$.[7] In other words, we are considering the selection near mean-field criticality and perturbative (in $j_{z\pm}$ and $j_{\pm\pm}$) vicinity of the U(1) symmetric portion of the theory [H_0 in Eq. (1a)]. Since we are focusing on the expansion of G in Eq. (10), we write its correction δG beyond the s-MFT solution as suggested by Eq. (8):

$$\delta G = 2\bar{\eta}_6(j_{\pm\pm}, j_{z\pm}) |m_{xy}|^6 \cos(6\phi). \quad (11)$$

As discussed in Sec. II A, $\bar{\eta}_6(j_{\pm\pm}, j_{z\pm}) = 0$ determines the phase boundaries between the ψ_2 and the ψ_3 states in the space of coupling constants $j_{\pm\pm}$ and $j_{z\pm}$. We now proceed to calculate $\bar{\eta}_6(j_{\pm\pm}, j_{z\pm})$ with the E-TAP method.

In the nth order of the β expansion, factors of the form $j_{\pm\pm}^k j_{z\pm}^l$ arise, where k and l are positive integers and $k + l = n$. Each power of $j_{\pm\pm}$ and $j_{z\pm}$ contributes factors of $e^{\pm 2i\phi}$ and $e^{\pm i\phi}$, respectively [see Eq. (1c)], to the corresponding term in the β expansion. By a simple power counting of these factors, one can pinpoint the terms that contribute to $\cos(6\phi)$ and $\cos(3\phi)$ that are necessary to compute due to their contribution to ω and η_6 and, consequently, to $\bar{\eta}_6$ (see. Eq. (9)), and which arise at different orders in β in the E-TAP calculation. It is straightforward arithmetic to find what combinations of k and l in $j_{\pm\pm}^k j_{z\pm}^l$ generate $\cos(6\phi)$ and $\cos(3\phi)$ terms. We then calculate ω and η_6 in Eqs. (5) and (6) in terms of the microscopic couplings $j_{\pm\pm}$ and $j_{z\pm}$ using the E-TAP method (see Appendix C). We obtain $\omega(j_{\pm\pm}, j_{z\pm})$, $\eta_6(j_{\pm\pm}, j_{z\pm})$, and thus $\bar{\eta}_6(j_{\pm\pm}, j_{z\pm})$, all to lowest nontrivial order in $j_{\pm\pm}$ and $j_{z\pm}$. These read as[8]

$$\begin{aligned} \omega(j_{\pm\pm}, j_{z\pm}) = {} & a_0 \beta j_{\pm\pm} j_{z\pm} + \beta^2 (a_1 j_{\pm\pm}^2 j_{z\pm} + a_2 j_{z\pm}^3) \\ & + \beta^3 (a_3 j_{\pm\pm}^3 j_{z\pm} + a_4 j_{\pm\pm} j_{z\pm}^3) \end{aligned} \quad (12)$$

and

$$\begin{aligned} \eta_6(j_{\pm\pm}, j_{z\pm}) = {} & b_0 \beta^2 j_{\pm\pm}^3 + b_1 \beta^3 j_{\pm\pm}^2 j_{z\pm}^2 \\ & + b_2 \beta^4 j_{\pm\pm} j_{z\pm}^4 + b_3 \beta^5 j_{z\pm}^6, \end{aligned} \quad (13)$$

[6] Considering $J_{zz} \neq 0$ contributions to the $\cos(6\phi)$ coefficient would require calculating higher-order terms in β in the expansion of Eq. (10). Such a calculation is beyond the scope of the present work.

[7] We recall that $J_\pm$ is the dominant interaction and $j_{\pm\pm}$ and $j_{z\pm}$ are being treated perturbatively in Eq. (1).

[8] We note that E-TAP corrections of the coefficient r_1 in Eq. (5) does not contribute to $\bar{\eta}_6(j_{\pm\pm}, j_{z\pm})$ when it is calculated to the lowest order in the coupling constants $j_{\pm\pm}$ and $j_{z\pm}$, and we therefore use its s-MFT $r_1 = 2/\beta$ value.

TABLE I. Values of a_i in $\omega(j_{\pm\pm}, j_{z\pm})$ multiplied by 10^2.

a_0	a_1	a_2	a_3	a_4
−0.593	−1.13	−0.451	−0.938	7.21

and, consequently,

$$2\bar{\eta}_6(j_{\pm\pm}, j_{z\pm}) = c_0\beta^2 j_{\pm\pm}^3 + c_1\beta^3 j_{\pm\pm}^2 j_{z\pm}^2 + c_2\beta^4 j_{\pm\pm} j_{z\pm}^4 + \beta^5(c_3 j_{\pm\pm}^4 j_{z\pm}^2 + c_4 j_{\pm\pm}^2 j_{z\pm}^4 + c_5 j_{z\pm}^6). \quad (14)$$

In Eqs. (12)–(14), a_i ($i = 0, \ldots, 4$), b_j ($j = 0, \ldots, 3$), and c_k ($k = 0, \ldots, 5$) are numerical coefficients determined by the explicit E-TAP calculation too lengthly to reproduce here, but whose derivation is described in Appendix C. Considering the highest power of coupling constants $j_{\pm\pm}$ and $j_{z\pm}$ in Eq. (14), one needs to compute terms up to sixth order in the high-temperature expansion of G in Eq. (10).

2. Results

In order to obtain the numerical value of the a_i, b_j, and c_k coefficients in Eq. (14), we employ a diagrammatic technique to represent the terms in the β expansion and which constitutes the computational core of the E-TAP method. These diagrams are composed of vertices and bonds [52]. The vertices correspond to lattice sites covered by a diagram and the bond represents the interaction between the vertices that it connects. The details necessary to carry out the calculations using diagrams are presented in Appendix C 4. As mentioned earlier, for computational simplicity, we only consider the case of $j_{zz} = 0$. Recalling Eq. (9), and noting that to the lowest order we can use the s-MFT value of r_1, $r_1 = 2/\beta$, we find

$$\begin{aligned} 2\bar{\eta}_6(j_{\pm\pm}, j_{z\pm}) = 10^{-5} \times \big[&-6.50\beta^2 j_{\pm\pm}^3 + 57.3\beta^3 j_{\pm\pm}^2 j_{z\pm}^2 \\ &+ 26.5\beta^4 j_{\pm\pm} j_{z\pm}^4 + 27.8\beta^5 j_{z\pm}^6 \\ &- 7.95\beta^5 j_{\pm\pm}^4 j_{z\pm}^2 - 4.60\beta^4 j_{\pm\pm}^3 j_{z\pm}^2 \\ &+ 66.5\beta^5 j_{\pm\pm}^2 j_{z\pm}^4\big]. \end{aligned} \quad (15)$$

In deriving Eq. (15), we used ω and η_6 in Eqs. (12) and (13), respectively, with the numerical values of a_i and b_j coefficients given in Tables I and II.

Since $\bar{\eta}_6(j_{\pm\pm}, j_{z\pm}) = 0$ determines the boundaries between the ψ_2 and ψ_3 states, we need to compute the roots of Eq. (15). In order to be consistent with the above E-TAP derivation perturbative in $j_{z\pm}$ and $j_{\pm\pm}$, we ought to only consider the lowest order term in the root of η_6 given by Eq. (15). We find that Eq. (15) has one real root which to, the lowest order in the coupling constants, reads

$$j_{\pm\pm} \approx p_0 j_{z\pm}^2 + \cdots, \quad (16)$$

where the $\cdots$ represent higher-order terms in $j_{z\pm}$ and $p_0 \approx 9.37\beta$, which determines the phase boundary between the

TABLE II. Values of b_j in $\eta_6(j_{\pm\pm}, j_{z\pm})$ multiplied by 10^4.

b_0	b_1	b_2	b_3
−0.322	2.92	1.42	1.42

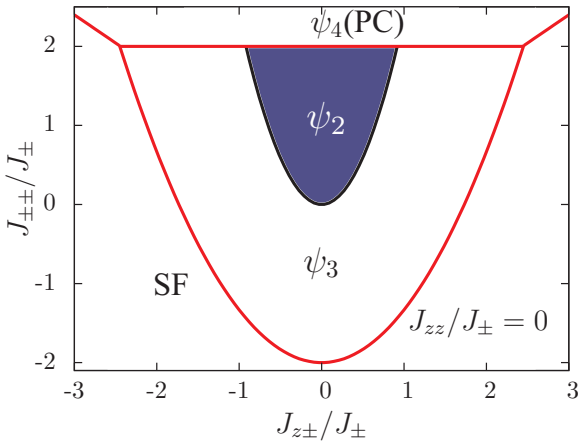

FIG. 2. (Color online) The $j_{zz} = 0$ phase diagram of the model at $T \lesssim T_c$. The Γ_5 region corresponds to the region enclosing the ψ_2 and ψ_3 states taken together. The Γ_5 region is circumscribed by an outer (red) parabola $j_{\pm\pm} = 2j_{z\pm}^2/3 - 2$ and a horizontal red line at $j_{\pm\pm} = 2$ obtained from the s-MFT calculation [17]. The phase boundary between the ψ_2/ψ_3 states obtained from the E-TAP calculations (i.e., the roots of $\bar{\eta}_6 = 0$, see text) is represented by the black line. The phases outside of the boundaries of the Γ_5 region are the following: a splayed ferromagnet (SF) [44] canted from the [100] cubic direction and the so-called ψ_4 or Palmer-Chalker (PC) state [17,26,53]. Both the SF and the PC phases have $\boldsymbol{k} = 0$ ordering wave vector.

ψ_2 and the ψ_3 states for $j_{zz} = 0$, $j_{z\pm} \ll 1$, and $\beta \gtrsim \beta_c$. The corresponding ψ_2-ψ_3 boundary for $\beta = 0.253 \gtrsim \beta_c^{\mathrm{MF}} = 1/4$, providing an estimate of the boundary in the limit $T \to T_c^-$, is shown Fig. 2. The "outer" s-MFT boundaries of the overall Γ_5 region for $j_{zz} = 0$ is also shown in this figure. Outside the Γ_5 boundary, the system orders in a Palmer-Chalker (PC) state [17,26,53] or a splayed ferromagnet (SF) [44].

It was found in Ref. [17] that, at zero-temperature, quantum fluctuations yield three distinct phase boundary for $j_{zz} = 0$, a result confirmed in Ref. [31], even in the regime $j_{z\pm} \ll 1$ and $j_{\pm\pm} \ll 1$, for which the E-TAP results for the ordered state selection at $T \lesssim T_c$ presented here apply. The combination of the E-TAP results with those from Ref. [17] suggests, because of the different ψ_2/ψ_3 boundaries at $T = T_c^-$ and $T = 0$, the possibility of multiple transitions between ψ_2 and ψ_3 as the temperature is decreased well below T_c as was found for the model of Ref. [33]. Such a multiple-transition scenario constitutes an exotic variant of the more conventional ObD phenomenon since fluctuations select distinct long-range ordered states in different temperature regimes ($T \lesssim T_c$ and $T = 0^+$). That being said, one should be reminded that since the E-TAP phase diagram of Fig. 2 was constructed on the basis of a *lowest order* fluctuation correction to s-MFT described by Eqs. (12)–(14) and for a classical version of $\mathcal{H}$ in Eq. (1), this discussion of multiple transitions is therefore only qualitative within the present E-TAP calculation. However, we expand further on this topic in Sec. IV within a Ginzburg-Landau theory framework. In the low-temperature regime, $T \ll T_c$, a study that incorporates high-order magnon-magnon interaction at nonzero temperature starting from the results of Ref. [17] would be of interest to explore this phenomenology further. This is, however, beyond the scope of the present work.

B. Cluster mean-field theory (c-MFT)

It is interesting to ask to what extent a calculation, any calculation, that goes beyond s-MFT may reveal an ordered state selection at $T \lesssim T_c$. For this reason, we study in this section the effect of fluctuations numerically using c-MFT. This method incorporates fluctuations at the level of one tetrahedron by exactly diagonalizing the Hamiltonian corresponding to the tetrahedron and treating the interactions between different tetrahedra at the s-MFT level. The c-MFT approach does not involve a perturbative scheme in powers of β compared with the E-TAP method where fluctuations are included through an expansion of the Gibbs free energy in powers of β [see Eq. (10)]. In c-MFT, fluctuations are limited to one tetrahedron while, in the E-TAP method, fluctuations beyond one tetrahedron are included up to the range spanned by the diagrams generating the sixth order terms in the high-temperature expansion of G (see Appendix C 4 for details). One practical advantage of the c-MFT method compared to the E-TAP approach is that c-MFT allows us to easily investigate the effect of nonzero J_{zz} on the selection of the ψ_2 versus the ψ_3 state. In what follows, we first provide the details of the c-MFT method and then present in Fig. 4 the results of the calculations for various J_{zz} values.

1. Method

The c-MFT that we use here may be viewed as a general, nonperturbative, and rather system-independent way to obtain (numerical) results beyond s-MFT. While the approach is not specific to the type of spins (classical or quantum) considered, we restrict ourselves to quantum spins 1/2 for a tetrahedron cluster. A pragmatic reason for using quantum spins here is to avoid the complicated eight integrals over the solid angle that correspond to the classical trace for classical spins taken as vectors of fixed length $|\boldsymbol{S}_i| = 1/2$ and orientation defined by an azimuthal and a polar angle. To illustrate the method, we write the model Hamiltonian (1) in the compact form:

$$\mathcal{H} = \sum_{\langle ij\rangle,\mu,\nu} J_{ij}^{\mu\nu} S_i^{\mu} S_j^{\nu}, \tag{17}$$

with $\mu,\nu = z, +, -$ and

$$J_{ij}^{\mu\nu} := \begin{pmatrix} J_{zz} & J_{z\pm}\zeta_{ij} & J_{z\pm}\zeta_{ij}^{*} \\ J_{z\pm}\zeta_{ij} & J_{\pm\pm}\gamma_{ij} & -J_{\pm} \\ J_{z\pm}\zeta_{ij}^{*} & -J_{\pm} & J_{\pm\pm}\gamma_{ij}^{*} \end{pmatrix}. \tag{18}$$

For N sites on the pyrochlore lattice, there are $N/4$ "up" and $N/4$ "down" corner-sharing tetrahedra (see Fig. 3). The diamond lattice, dual to the pyrochlore lattice, offers a simple representation of the tetrahedra that tessellate the lattice as elementary units. We note that the diamond lattice is bipartite (it is composed of 2 fcc sublattices, say A and B). As we consider ordered phases with a $\boldsymbol{k} = 0$ ordering wave vector, we assume in the c-MFT method that all tetrahedra on sublattice A are equivalent and interact with each other only through the mean fields. We re-express model (17) in a more suggestive form as a sum over sublattice A (labelled with I or I') and take $i,j = 1,2,3,4$ as the sublattice indices:

$$\mathcal{H} = \sum_{I\in A}\sum_{\langle ij\rangle,\mu,\nu} J_{ij}^{\mu\nu} S_{i,I}^{\mu} S_{j,I}^{\nu} + \sum_{\langle I,I'\rangle\in A}\sum_{\langle ij\rangle,\mu,\nu} J_{ij}^{\mu\nu} S_{i,I}^{\mu} S_{j,I'}^{\nu}. \tag{19}$$

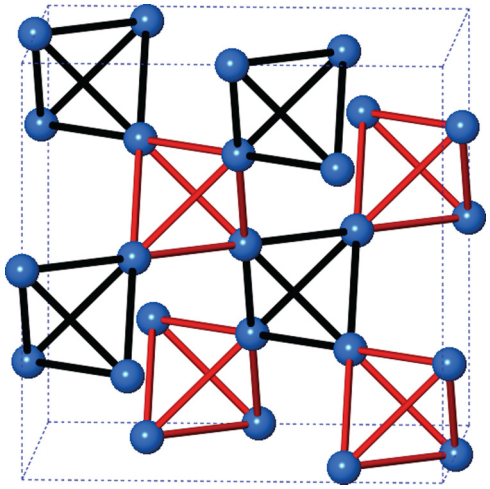

FIG. 3. (Color online) The pyrochlore lattice, with spins located at the vertices of corner-sharing tetrahedra. There are two orientations of tetrahedra indicated by the black and red colored tetrahedra with the interaction paths represented by the colored lines. The centers of the tetrahedra form a diamond lattice (with sublattice A and B corresponding respectively to, say, the black and red tetrahedra). In c-MFT, the interaction in-between the black tetrahedra is treated at the mean-field theory level.

We then proceed to apply a s-MFT approximation *only* on the second term of Eq. (19): we neglect any fluctuations *between* the A tetrahedra while taking full account of fluctuations *within* the A tetrahedra. The self-consistently determined mean fields $\langle S_{i,I}^{\mu}\rangle \equiv m_{i,I}$ are introduced to decouple the intercluster bonds. Again, because we focus on the Γ_5 manifold with $\boldsymbol{k} = 0$ ordering wave vector, we have translational invariance of sublattice A, which implies $m_{i,I'}^{\nu} = m_{i,I}^{\nu}$. By performing this approximation, Eq. (19) reduces to a sum over the A tetrahedra coupled together by the mean fields:

$$\mathcal{H}_{\rm MF} = \sum_{I\in A}\sum_{i,j,\mu,\nu} J_{ij}^{\mu\nu} \times \left(\frac{1}{2} S_{i,I}^{\mu} S_{j,I}^{\nu} + S_{i,I}^{\mu} m_{j,I}^{\nu} - \frac{1}{2} m_{i,I}^{\mu} m_{j,I}^{\nu}\right). \tag{20}$$

Any thermodynamic average is readily computed from $\mathcal{H}_{\rm MF}$. In particular, it is straightforward to show that the physical solution $\{m_i^{\mu}\}$ that minimizes the free energy corresponds to $m_i^{\mu} = \langle S_i^{\mu}\rangle$, where the thermodynamic average is taken with respect to the cluster mean-field Hamiltonian $\mathcal{H}_{\rm MF}$. While we focus on the $|\boldsymbol{S}_i| = 1/2$ case, we note that c-MFT could be used for $|\boldsymbol{S}_i| > 1/2$ and extended to clusters with more than four spins. The method (using quantum spins) is only constrained by the computational limitations of the required exact full diagonalization over the cluster considered [54].

2. Results

The critical temperature T_c is a function of the $J_{\pm}$, $J_{z\pm}$, and $J_{\pm\pm}$ exchange parameters. For every point in the phase diagrams (i.e., for a given set of exchange couplings $j_{z\pm}$ and $j_{\pm\pm}$), we determine T_c by identifying the temperature at which there is a minimum of the free energy and the development of a numerically nonzero on-site magnetization

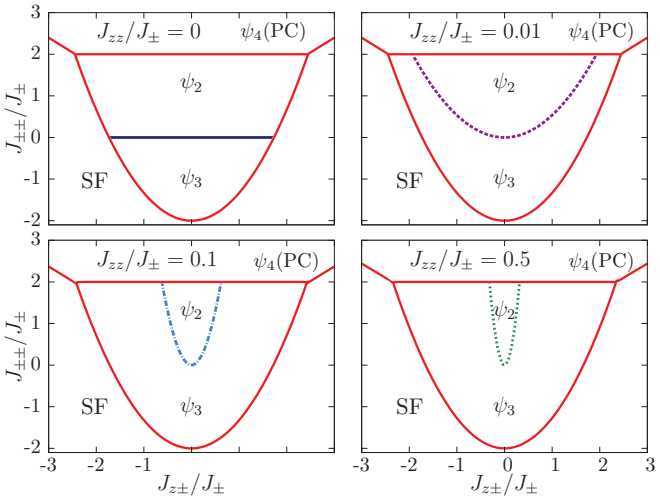

FIG. 4. (Color online) The c-MFT phase diagram at $T \lesssim T_c$ obtained for positive $j_{zz} = 0.5, 0.1, 0.01, 0$. The region circumscribed by the red line is the ψ_2/ψ_3 Γ_5 region. For a given phase boundary (fixed j_{zz}), the area above (below) that phase boundary line corresponds to the ψ_2 (ψ_3) phase. The phase boundaries for negative values of j_{zz} will be approximately a reflection of the presented phase boundaries with respect to the $j_{zz} = 0$ line. Again, the phases outside of the boundaries of the Γ_5 region are: a splayed ferromagnet (SF) canted from the [100] cubic direction [44] and the so-called ψ_4 [26] or Palmer-Chalker (PC) state [53].

$\boldsymbol{m}$. For definitiveness, we then take a temperature slightly below T_c, $T = 0.9T_c$, for each $(j_{z\pm}, j_{\pm\pm})$ and determine which state (ψ_2 or ψ_3) is selected. We record this state selection over a grid of points that span the Γ_5 manifold.

The c-MFT ψ_2/ψ_3 phase boundary obtained for various j_{zz} values is presented in Fig. 4. The previous symmetry analysis in Sec. II A of the Γ_5 manifold showed that a nonzero m_z component is only compatible with the ψ_2 state. As a corollary and confirmation of this expectation, we observe that as j_{zz} is varied, the ψ_2/ψ_3 phase boundary position shifts. This can be understood physically in the following way. A negative j_{zz} favors a "4-in/4-out" hence nonzero m_z and thus the ψ_2 state. Conversely, a positive j_{zz} on a single tetrahedron alone would favor a "2-in/2-out" spin configuration and therefore disfavor a 4-in/4-out configuration. However, an ordered state built with such 2-in/2-out spin configuration would have a nonzero net magnetization on each tetrahedron, as well as for the whole system since we consider a $\boldsymbol{k} = 0$ propagation vector, which is forbidden for the Γ_5 representation under discussion. Therefore, the best that a positive j_{zz} can do is to favor the ψ_3 state ($m_z = 0$) against ψ_2 ($m_z \neq 0$) and the boundary shifts accordingly, as shown in Fig. 4.

A comment is warranted regarding the flat ($J_{z\pm}$–independent) ψ_2/ψ_3 phase boundary predicted by c-MFT for $J_{zz} = 0$ in Fig. 4. This is to be contrasted with the E-TAP results of Fig. 2 and the $T = 0$ quantum fluctuation calculations of Ref. [17] (see Fig. 3 therein), which both show a $J_{z\pm}$-dependent ψ_2-ψ_3 phase boundary for $J_{zz} = 0$. This $J_{z\pm}$ independent c-MFT result can be rationalized in the following way with the argument proceeding through a sequence of steps. In the c-MFT approximation that considers a one-tetrahedron cluster, the m_z dependence of the free energy comes only from the J_{zz} term because of the special role the C_3 symmetry plays when considering such a cluster. The reason is that every spin on a one-tetrahedron cluster is coupled to three idential "exterior" mean fields $\boldsymbol{m}_{j,I}$ because of the $\boldsymbol{k} = 0$ ψ_2 or ψ_3 long-range ordered states considered. As a result, terms such as $(\sum_i S_i^\pm)(\sum_j \zeta_{ij} m_{j,I}^z)$ vanish due to the C_3 symmetry that imposes the necessary form for the ζ_{ij} bond factors [16,44,48]. The same argument of course applies for terms of the form $(\sum_i m_{i,I}^\pm)(\sum_j \zeta_{ij} S_j^z)$. Consequently, the free energy depends on m^z explicitly only via the J_{zz} coupling since the combined dependence on $J_{z\pm}$ and m^z is eliminated via the above argument. When $J_{zz} = 0$, all dependence of the c-MFT free energy on m^z disappears, and thus no-dependence on $J_{z\pm}$ can remain, as found in Fig. 4. On the other hand, when $J_{zz} \neq 0$, the c-MFT free energy depends on m^z. In that case, $J_{z\pm}$ coupling the S_i^z and $S_i^\pm$ components will, through the *intratetrahedra* fluctuations that are incorporated into the c-MFT calculation, renormalize the effective intratetrahedron zz component sublattice susceptibility and thus the net effect of *intertetrahedra* mean field $(\sum_j J_{zz} m_{j,J}^z)$. As a result, for $J_{zz} \neq 0$, a $J_{z\pm}$ dependence of the ψ_2/ψ_3 phase boundary is observed for a single-tetrahedron c-MFT calculation (see Fig. 4).

While the above argument for the $J_{z\pm}$ independence of the boundary for the $J_{zz} = 0$ case applies for a single tetrahedron cluster c-MFT, we expect the boundary for larger clusters to depend on $J_{z\pm}$, even for $J_{zz} = 0$. In that case, $J_{z\pm}$ may induce a m^z dependence that would result in a behavior similar to E-TAP results for $J_{zz} = 0$. The reason is that, for larger clusters, the sites on the perimeter of the cluster may be coupled to the mean-field parameters $\boldsymbol{m}_{j,I}$ coming from less than three sites related by C_3 symmetry, and which caused the intertetrahedron mean field to vanish for a four-site tetrahedron cluster as discussed above. Notwithstanding this caveat associated with the special symmetry of the four-site tetrahedron cluster, we nevertheless believe that the evolution of the boundary upon varying J_{zz} shown in Fig. 4 to be roughly qualitatively correct for $J_{zz} \neq 0$.

IV. MULTIPLE TRANSITIONS AT $T < T_c$

The results above, along with those of Refs. [17,31], suggest that in some circumstances the state selected at T_c may differ from the low-temperature phase selected by harmonic (classical or quantum) spin waves. For example, Ref. [33] found that, in a classical pyrochlore Heisenberg antiferromagnet with additional indirect Dzyaloshinskii-Moriya interaction, the state selected at $T \lesssim T_c$ is ψ_2, while the one selected at $T = 0^+$ is ψ_3. One might then ask what are the generic possibilities that may occur in xy pyrochlore magnets for which the anisotropic exchange terms position them in the degenerate Γ_5 manifold. Considering the lowest-order term in m_{xy}, one has, as discussed above in Sec. II A,

$$\delta\mathcal{F}_{\rm GL}(\phi) = f_6(T)\cos(6\phi). \tag{21}$$

$f_6(T) \equiv 2\bar{\eta}_6 |m_{xy}|^6$ is a function of temperature, T, for fixed anisotropic exchange terms $J_\pm$, J_{zz}, $J_{z\pm}$, and $J_{\pm\pm}$, with the sign of $f_6(T)$ dictating which state is selected at a given temperature. If $f_6(T = 0^+)$ stays of the same sign for all

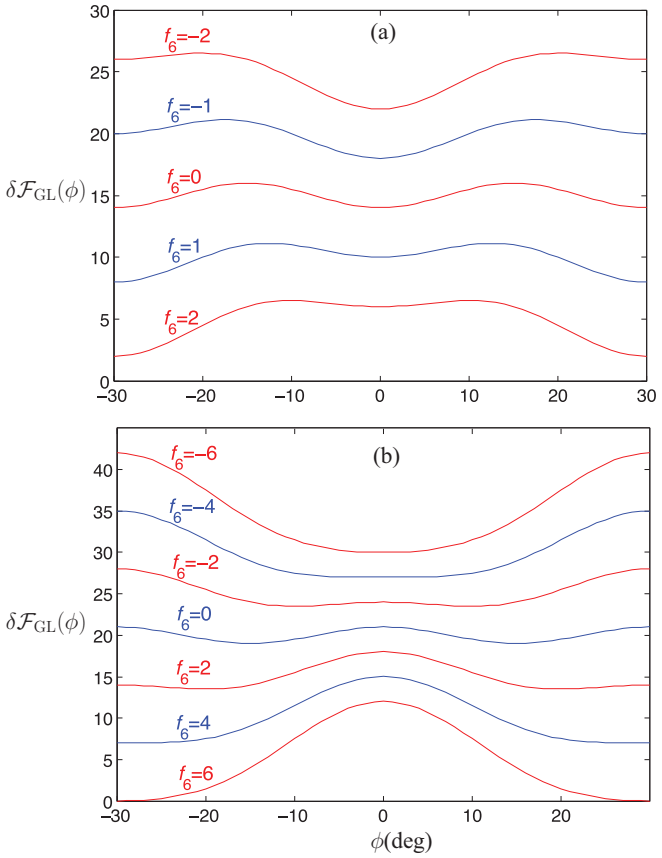

FIG. 5. (Color online) (a) Sequence of $\delta\mathcal{F}_{\rm GL}(\phi)$ with $f_{12}=-1$ and $f_6=-2$, -1, 0, 1, and 2 (from top to bottom). There is a first-order transition at $f_6=0$. (b) Sequence of $\delta\mathcal{F}_{\rm GL}(\phi)$ with $f_{12}=1$ and $f_6=-6$, -4, -2, 0, 2, 4, and 6 (from top to bottom). In mean-field theory, there are Ising-type second-order transitions at $f_6=\pm 4|f_{12}|$.

$0<T<T_c$, only a single phase is realized below T_c. With solely this lowest-order anisotropic term in $\delta\mathcal{F}_{\rm GL}$, the only other possibility is a first order transition between ψ_2 and ψ_3 at some temperature $T^*<T_c$ when $f_6(T)$ changes sign at $T=T^*$. However, as one gets far below T_c, higher-order terms in $|m_{xy}|$ can become of significant magnitude in $\mathcal{F}_{\rm GL}$. One may then extend the Ginzburg-Landau free energy by incorporating higher-order harmonics in the anisotropy potential as

$$\delta\mathcal{F}_{\rm GL}(\phi)=\sum_{n=1}2\bar{\eta}_{6n}(T)|m_{xy}|^{6n}\cos(6n\phi). \tag{22}$$

Keeping only the two lowest-order terms for illustration purposes, we have

$$\delta\mathcal{F}_{\rm GL}(\phi)=f_6(T)\cos(6\phi)+f_{12}(T)\cos(12\phi), \tag{23}$$

where $f_{6n}\equiv 2\bar{\eta}_{6n}|m_{xy}|^{6n}$. For simplicity, consider first $f_{12}=-1$ As $f_6(T)$ varies from $f_6(T)<0$ to $f_6(T)>0$, a first-order transition occurs when the minimum of $\delta\mathcal{F}_{\rm GL}$ shifts discontinuously, in a first-order transition, from $\phi=0$ (ψ_2 state) to $\phi=\pi/6$ (ψ_3 state) [see Fig. 5(a)]. A more interesting behavior is in principle possible. Consider now $f_{12}=+1$. In that case, second-order (Ising-type) transitions occur at $f_6=\pm 4|f_{12}|$. For example, for $f_6<-4$, the minimum is at $\phi=0$ (a ψ_2 state), and a second order transition to a f_6-dependent angle ϕ occurs at $f_6=-4$. As f_6 continues growing and become less negative (at fixed $f_{12}=+1$), the magnetic moment orientation ϕ continues increasing until another second-order transition to the ψ_3 state occurs at $f_6=+4$ [see Fig. 5(b)]. While the direct ψ_2 to ψ_3 transition observed in the pyrochlore Heisenberg antiferromagnet with indirect Dzyaloshinskii-Moriya interaction [33] suggests that this system belongs to the first case, the second scenario is perhaps not excluded in more complex models in which both temperature and applied magnetic field are varied simultaneously, or when the magnetic Er^{3+} sites are diluted by nonmagnetic ions [55,56].

In the above discussion, we have implicitly assumed that the anisotropic terms $[m_z(m_{xy})^3+\text{c.c.}]^k$ and $[(m_{xy})^6+\text{c.c.}]^l$, which give terms of the form $|m_{xy}|^{6n}\cos(6n\phi)$ in the Ginzburg-Landau theory once m_z has been eliminated (see discussion in Sec. II A), are generated by thermal fluctuations beyond the Ginzburg-Landau free energy derived by a s-MFT treatment of the microscopic model $\mathcal{H}$ in Eq. (1). However, it is, in principle, possible that virtual crystal-field excitations (VCFE) [30,43,45,46] mediated by the bare multipolar interactions between the rare-earth ions would generate [30,57] an effective pseudospin-1/2 Hamiltonian more complex than the one given by Eqs. (1a), (1b), and (1c) and involve multispin (e.g., ring-exchange-like) interactions capable of lifting degeneracy at the classical level without invoking order-by-disorder [15,16]. However, one naively expects those interactions generated by VCFE to be significantly smaller compared with the $J_\pm$, $J_{\pm\pm}$, $J_{z\pm}$, and J_{zz} of Eq. (1a), as stated in Ref. [16]. Whether those terms are truly inefficient in competing with order-by-disorder, once the commonly large prefactors of combinatoric origin arising in high-order perturbation theory have been taken into account, must await a detailed calculation.

V. DISCUSSION

In this work, we first used an extended TAP (E-TAP) method to analytically study the problem of order-by-disorder (ObD) near the critical temperature of a general three-dimensional xy antiferromagnetic model on the pyrochlore lattice with the Hamiltonian (1) with $J_{zz}=0$. We focused on the Γ_5 manifold, which is U(1) degenerate at the standard mean-field theory (s-MFT) level. The fluctuations corrections to the free energy beyond s-MFT were organized as an expansion in powers of the inverse temperature, β, and to lowest orders in the coupling constants $j_{\pm\pm}=J_{\pm\pm}/J_\pm$, $j_{z\pm}=J_{z\pm}/J_\pm$ and the on-site magnetization $\boldsymbol{m}$. We established that in different parts of the Γ_5 region, the ψ_2 and ψ_3 states are the only minima of the free energy selected by fluctuations up to the lowest-order U(1) symmetry-breaking terms considered. The phase boundary between ψ_2 and ψ_3 can then be obtained by finding the real roots of Eq. (14) in terms of $J_{\pm\pm}/J_\pm$ and $J_{z\pm}/J_\pm$. We also numerically studied the ObD mechanism in the 3D-xy pyrochlore system using a cluster mean-field theory (c-MFT). Using this method, we obtained a phase boundary between ψ_2 and ψ_3 states for a variety of J_{zz} values shown in Fig. 4.

Using a Ginzburg-Landau theory, along with E-TAP and c-MFT calculations, we predict that for a state ordered in the local xy plane at the s-MFT level, fluctuations can induce a small out-of-xy-plane m_z component of the on-site

magnetization. This fluctuation-induced local z component of the magnetization is only compatible with the ψ_2 state. We expect the size of this moment to be small, since it is proportional to $|m_{xy}|^3 \ll 1$ for $T \lesssim T_c^{\rm MF}$ [see Eq. (7)]. Yet, on the basis of the c-MFT results, we might anticipate that nonzero m_z has an important effect on the phase boundary between the ψ_2 and the ψ_3 states for $J_{zz} \neq 0$, as illustrated in Fig. 4 (see also the caption of the figure).

By considering the single phase boundary between the ψ_2 and ψ_3 states for $T \lesssim T_c$ along with the multiple ψ_2-ψ_3 boundaries found at $T = 0^+$ in Ref. [17], for $j_{\pm\pm} \ll 1$ and $j_{z\pm} \ll 1$, the regime for which the perturbative E-TAP solutions above apply, one may expect to find multiple phase transitions between ψ_2 and ψ_3 states upon decreasing temperature from $T \lesssim T_c$ to $T \sim 0^+$. While possible in principle and found in a numerical study [33], such multiple transitions in real xy pyrochlore magnetic materials have not yet been reported. Since in the E-TAP calculations the $j_{\pm\pm}$ and $j_{z\pm}$ couplings were treated perturbatively, the E-TAP phase boundary in Eq. (16) is valid for small $j_{\pm\pm}$ and $j_{z\pm}$ and would thus need to be modified for nonperturbative $j_{\pm\pm}$ and $j_{z\pm}$, that is, closer to the boundaries of the Γ_5 region with the splayed-ferromagnet (SF) phase (see Fig. 2). A case in point is the Heisenberg pyrochlore antiferromagnet with indirect Dzyaloshinskii-Moriya interaction [33]. This model displays a transition at T_c^+ from a paramagnetic state to ψ_2, followed at $T_c^- < T_c^+$ by a transition from ψ_2 to ψ_3 [33], and for which the corresponding anisotropic exchange $J_\pm$, $J_{\pm\pm}$, $J_{z\pm}$, and J_{zz} are such that this model lives *right on* the Γ_5 to SF classical phase boundary [17].

The difference between the phase boundaries obtained by E-TAP and c-MFT for $J_{zz} = 0$ (see Figs. 2 and 4) arises from the different range of fluctuations considered in these two methods. In c-MFT, because of the exact diagonalization of the Hamiltonian on a single tetrahedron and the s-MFT treatment of the intertetrahedra couplings, the fluctuation corrections considered are short-ranged (limited to the nearest-neighbors). However, in the E-TAP method, by considering the higher-order terms in the β expansion, specifically β^4 and beyond where larger (more extended) diagrams appear in the calculation (see Appendix C, Sec. C 4), fluctuations beyond nearest-neighbors are included. It would be of interest to benchmark these arguments by performing c-MFT calculations for larger clusters.

The E-TAP corrections to the s-MFT free energy could also be computed for the $J_{zz} \neq 0$ case. The procedure for considering $J_{zz} \neq 0$ is conceptually the same as for the $J_{zz} = 0$ case for which, using the E-TAP method, we calculated the terms in the high temperature expansion of Eq. (10) that contribute to the degeneracy-lifting $\cos(3\phi)$ and $\cos(6\phi)$ terms in the free energy. To obtain these terms to the lowest order in the coupling constants $J_{\pm\pm}$, $J_{z\pm}$, and J_{zz}, one would need to consider the high temperature expansion of G up to the seventh order in β and calculate the degeneracy lifting terms following the power-counting prescription explained above Eq. (12). However, the number of terms of the form $j_{zz}^l j_{\pm\pm}^m j_{z\pm}^n$, with fixed $l + m + n$ value l, m, and n positive integers, and thus the number of diagrams to be computed, proliferate significantly as to make this calculation a significant undertaking. The $J_{zz} \neq 0$ case thus stands on its own as an independent future study.

Finally, we remark that variants of the E-TAP method presented in this work could be applied to models other than the pyrochlore structure to analytically investigate the role of fluctuations beyond s-MFT in selecting a specific long-range ordered state close to the critical temperature. One example is the case of Heisenberg spins on face centered cubic (fcc) lattice interacting via magnetostatic dipole-dipole interaction [58,59]. Generally speaking, one might expect that a consideration of an E-TAP analytical description of fluctuations at the microscopic level may help shed light on the role of individual symmetry-allowed interactions in the ordered state selection near the critical temperature over a broad range of frustrated spins models for which an accidental degeneracy exists in a standard mean-field theory description.

ACKNOWLEDGMENTS

We acknowledge Paul McClarty, Ludovic Jaubert, Jaan Oitmaa, Rajiv Singh, and Anson Wong for useful discussions and collaborations related to this work. We also thank Antoine Georges for a useful discussion. We are grateful to Peter Holdsworth and Natalia Perkins for constructive comments and suggestions on an earlier version of the manuscript. This work was supported by the NSERC of Canada, the Canada Research Chair program (M.G., Tier 1) and by the Perimeter Institute (PI) for Theoretical Physics. Research at PI is supported by the Government of Canada through Industry Canada and by the Province of Ontario through the Ministry of Economic Development & Innovation.

APPENDIX A: ψ_2 AND ψ_3 STATES

The ψ_2 states have spin configurations with a $\boldsymbol{k} = 0$ ordering wave vector and with the following spin orientations on a tetrahedron expressed in the global (Cartesian) reference frame:

$$\hat{e}_0^1 = \frac{1}{\sqrt{6}}(-1,-1,2), \tag{A1a}$$

$$\hat{e}_1^1 = \frac{1}{\sqrt{6}}(1,1,2), \tag{A1b}$$

$$\hat{e}_2^1 = \frac{1}{\sqrt{6}}(1,-1,-2), \tag{A1c}$$

$$\hat{e}_3^1 = \frac{1}{\sqrt{6}}(-1,1,-2). \tag{A1d}$$

Here, the subscripts correspond to the four sublattice labels in the pyrochlore lattice and the superscripts refer to different symmetry-related ψ_2 states. $\{\hat{e}_i^2\}$ and $\{\hat{e}_i^3\}$, $i = 0,\ldots,3$, can be obtained from Eq. (A1) by C_3 $(\pi/3)$ rotations with respect to the $\langle 111\rangle$ directions. ψ_3 states can be obtained from the ψ_2 ones, by a $\pi/6$ rotation of each spin about its local [111] axis.

APPENDIX B: SYMMETRY GROUPS OF ψ_2 AND ψ_3 STATES

The symmetries of either ψ_i state $(i = 2,3)$ form a group known as the little group of the corresponding state. The generators of the ψ_3 little group include the C_2 rotation by π about one of the cubic x, y or z axes (depending on the

particular ψ_3 state), the improper rotation by $\pi/2$ (S_4) about the same cubic axis, and two plane reflections σ_1 and σ_2 with respect to planes spanned by the cubic axis and one of the two tetrahedron bonds perpendicular to the cubic axis. The generators of the little group of ψ_2 states include τS_4, $\tau\sigma_1$, and $\tau\sigma_2$ where τ is the time-reversal symmetry operation.

Considering the action of the symmetry operations in the ψ_2's and ψ_3's little groups on the possible configurations with a finite onsite m_z moments on a single tetrahedron (i.e., all-in/all-out, 2-in/2-out, 3-in/1-out, and 1-in/3-out where "in" and "out" indicates whether $m_{i,z}$ is positive or negative on site i), only all-in-all-out configuration is invariant under the symmetry operations of the ψ_2's little group while none of the above configurations are invariant under the ψ_3's little group symmetry operations. As a result, only the ψ_2 state can possess a finite onsite m_z moment which displays an all-in-all-out configuration on a single tetrahedron and therefore does not produce a net magnetic moment on a tetrahedron.

APPENDIX C: EXTENDED TAP METHOD (E-TAP)

In this appendix, we first derive the general form of the E-TAP corrections up to sixth order in β. Next, we illustrate our method for calculating the terms in the β expansion of the Gibbs free energy, G, of Eq. (10) by focusing on two calculation examples. Finally, we discuss the general properties of the diagrammatic approach employed to carry out the computation of the various terms entering the E-TAP calculation.

1. Derivation

The E-TAP method is based on a perturbative expansion of the Gibbs free energy as a function of inverse temperature, β, beyond that given by s-MFT. There are several ways of deriving these corrections [60]. Here, we employ and extend the method presented by Georges and Yedidia [40] for Ising spin glass, which provides the corrections due to fluctuations about the s-MFT solution, order by order in β. In this part of the appendix, we focus on a temperature regime close to the mean-field transition temperature, $T \lesssim T_c^{\mathrm{MF}}$, and derive the E-TAP corrections for classical Heisenberg spins of fixed length $|\boldsymbol{S}| = 1/2$.

The Hamiltonian in Eq. (1), $\mathcal{H}$, can be written as

$$\mathcal{H} = \sum_{i<j} S_i^\mu J_{ij}^{\mu\nu} S_j^\nu, \tag{C1}$$

greek labels represent Cartesian coordinates and implicit summation over repeated superscripts is used. A Taylor series expansion of Eq. (10) in powers of β reads

$$G(\beta) = \frac{1}{\beta}\left[\tilde{G}(\beta)\Big|_{\beta=0} + \frac{\partial\tilde{G}(\beta)}{\partial\beta}\Big|_{\beta=0}\beta + \frac{1}{2!}\frac{\partial^2\tilde{G}(\beta)}{\partial\beta^2}\Big|_{\beta=0}\beta^2\cdots\right], \tag{C2}$$

where $\tilde{G}(\beta) = \beta G(\beta)$. We define

$$U \equiv \frac{1}{2}\sum_{ij} \delta S_i^\mu J_{ij}^{\mu\nu} \delta S_j^\nu, \tag{C3}$$

where

$$\delta S_j^\nu \equiv S_j^\nu - m_j^\nu \tag{C4}$$

are spin fluctuations about the s-MFT solution. As shown in Ref. [40], the derivatives of $\tilde{G}(\beta)$ with respect to β can be evaluated in terms of expectation values of powers of U and T_n, that read

$$\frac{\partial(\beta G(\beta))}{\partial\beta} = \langle\mathcal{H}\rangle, \tag{C5a}$$

$$\frac{\partial^2(\beta G(\beta))}{\partial\beta^2} = -\langle U^2\rangle, \tag{C5b}$$

$$\frac{\partial^3(\beta G(\beta))}{\partial\beta^3} = \langle U^3\rangle, \tag{C5c}$$

$$\frac{\partial^4(\beta G(\beta))}{\partial\beta^4} = -\langle U^4\rangle + 3\langle U^2\rangle^2 - 3\langle U^2 T_2\rangle, \tag{C5d}$$

$$\frac{\partial^5(\beta G(\beta))}{\partial\beta^5} = \langle U^5\rangle - 10\langle U^2\rangle\langle U^3\rangle - 3\langle U^2 T_3\rangle + 7\langle U^3 T_2\rangle + 6\langle U T_2^2\rangle, \tag{C5e}$$

$$\frac{\partial^6(\beta G(\beta))}{\partial\beta^6} = -\langle U^6\rangle + 15\langle U^4\rangle\langle U^2\rangle + 10\langle U^3\rangle^2 - 30\langle U^2\rangle^3 - 12\langle U^4 T_2\rangle + 10\langle U^3 T_3\rangle - 3\langle U^2 T_4\rangle - 27\langle U^2 T_2^2\rangle + 18\langle U T_2 T_3\rangle - 6\langle U T_3\rangle\langle U^2\rangle + 51\langle U^2\rangle\langle U^2 T_2\rangle + 6\langle U^2\rangle\langle T_2^2\rangle - 6\langle T_2^3\rangle, \tag{C5f}$$

and where T_n is defined as

$$T_n \equiv \sum_i \frac{\partial^n \boldsymbol{\lambda}_i}{\partial\beta^n}\cdot\delta\boldsymbol{S_i}. \tag{C6}$$

Since $\partial\boldsymbol{\lambda}/\partial\beta|_{\beta=0} = \boldsymbol{h}_i$[40], where $h_i^\mu = \sum_{j,\nu} J_{ij}^{\mu\nu} m_j^\nu$, the terms involving involving T_n come from considering fluctuations of the local mean field. On the other hand, the U^n terms take into accont the fluctuations of the on-site magnetization [see Eqs. (C3) and (C4)] within the ensemble set by the s-MFT solution. The $\langle\cdots\rangle$ above denotes a thermal average. For a general observable O, $\langle O\rangle$ is given by

$$\langle O\rangle = \frac{\mathrm{Tr}[O\exp(-\beta H + \sum_i \boldsymbol{\lambda}_i\cdot(\boldsymbol{S_i} - \boldsymbol{m_i}))]}{\mathrm{Tr}[\exp(-\beta H + \sum_i \boldsymbol{\lambda}_i\cdot(\boldsymbol{S_i} - \boldsymbol{m_i}))]}. \tag{C7}$$

The first two terms in Eq. (C2) correspond to the s-MFT free energy, while the higher-order terms in β provide corrections beyond s-MFT. Calculating the expectation value of powers of U at $\beta = 0$ reduces to the evaluation of mean-field averages of the form

$$\langle\delta S_{i_1}^{\alpha_1}\delta S_{i_2}^{\alpha_2}\cdots\delta S_{i_n}^{\alpha_n}\rangle_{\mathrm{MF}}, \tag{C8}$$

where i_n represents the site label and α_n represents a Cartesian coordinate. n is the number of δS factors in Eq. (C8). From now on, we drop the MF subscript for compactness of notation. For $n = 1$, the expectation value in Eq. (C8) is zero due to the relation $\boldsymbol{m_i} = \langle\boldsymbol{S_i}\rangle$. For $n \geqslant 2$, however, Eq. (C8) is nonzero only if there is no site label that appears only once. For example, averages of the following form have a nonzero

contribution:

$$\left\langle \delta S_i^{\alpha_1} \delta S_i^{\alpha_2} \delta S_j^{\alpha_3} \delta S_j^{\alpha_4} \delta S_j^{\alpha_5} \right\rangle = \left\langle \delta S_i^{\alpha_1} \delta S_i^{\alpha_2} \right\rangle \left\langle \delta S_j^{\alpha_3} \delta S_j^{\alpha_4} \delta S_j^{\alpha_5} \right\rangle. \quad \text{(C9)}$$

The expectation values above can be calculated using the self-consistent s-MFT equations for three-component classical spins, which are given by the Langevin function,

$$\boldsymbol{m}_i = \frac{\boldsymbol{\lambda}_i}{|\boldsymbol{\lambda}_i|} \left[\coth(|\boldsymbol{\lambda}_i|) - \frac{1}{|\boldsymbol{\lambda}_i|} \right]. \quad \text{(C10)}$$

Consequently,

$$\left\langle \delta S_i^{\alpha} \delta S_i^{\beta} \right\rangle = \frac{\partial m_i^{\alpha}}{\partial \lambda_i^{\beta}} \equiv \chi_i^{\alpha\beta}, \quad \text{(C11)}$$

$$\left\langle \delta S_i^{\alpha} \delta S_i^{\beta} \delta S_i^{\gamma} \right\rangle = \frac{\partial \chi_i^{\alpha\beta}}{\partial \lambda_i^{\gamma}}, \quad \text{(C12)}$$

and, in general,

$$\left\langle \delta S_i^{\alpha_1} \delta S_i^{\alpha_2} \cdots \delta S_i^{\alpha_n} \right\rangle = \frac{\partial \left\langle \delta S_i^{\alpha_1} \delta S_i^{\alpha_2} \cdots \delta S_i^{\alpha_{n-1}} \right\rangle}{\partial \lambda_i^{\alpha_n}}. \quad \text{(C13)}$$

Since we are interested in a temperature range close to T_c, Eq. (C10) can be expanded for small $|\boldsymbol{\lambda}_i|$:

$$m_i^{\alpha} = \frac{\lambda_i^{\alpha}}{3} \left[1 - \frac{(|\boldsymbol{\lambda}_i|)^2}{15} + \frac{2(|\boldsymbol{\lambda}_i|)^4}{315} + \cdots \right], \quad \text{(C14)}$$

The expansions of Eqs. (C11)–(C13) at $T \lesssim T_c$ can be computed by differentiating Eq. (C14) with respect to different components of the vector $\boldsymbol{\lambda}_i$ Lagrange multipler.

In the rest of this section, we focus on the specific problem of the s-MFT U(1) degeneracy of the Γ_5 manifold displayed by the Hamiltonian of Eq. (1) in a wide range of the $\{J_{\pm}, J_{\pm\pm}, J_{z\pm}, J_{zz}\}$ anisotropic exchange parameters [17]. Below, we calculate the degeneracy-lifting contributions from $\langle U^2 \rangle$ and $\langle U^2 T_2 \rangle$ in Eqs. (C5b) and (C5d) to demonstrate the general idea of the method. Higher order terms can be calculated using a similar procedure.

2. $\langle U^2 \rangle$ Calculation

Using Eq. (C3), we have

$$\langle U^2 \rangle = \frac{1}{2^2} \sum_{\langle i_1, j_1 \rangle} \sum_{\langle i_2, j_2 \rangle} J_{i_1 j_1}^{\alpha_1 \beta_1} J_{i_2 j_2}^{\alpha_2 \beta_2} \left\langle \delta S_{i_1}^{\alpha_1} \delta S_{j_1}^{\beta_1} \delta S_{i_2}^{\alpha_2} \delta S_{j_2}^{\beta_2} \right\rangle, \quad \text{(C15)}$$

where the summations are performed over lattice sites and summation is implied for greek superscripts. To proceed, we need to specify all the possible pairings of the factors $\delta S_{i_t}, \delta S_{j_t}$ ($t = 1,2$) in the $\langle \delta S_{i_1}^{\alpha_1} \delta S_{j_1}^{\beta_1} \delta S_{i_2}^{\alpha_2} \delta S_{j_2}^{\beta_2} \rangle$.

Considering the description provided above Eq. (C9), the only nonzero pairings of site indices in Eq. (C15) are $i_1 = i_2$, $j_1 = j_2$ and $i_1 = j_2$, $j_1 = i_2$, with the constraint $i_1 \neq j_1$ and $i_2 \neq j_2$ imposed by the Hamiltonian; $J_{ii}^{\alpha\beta} = 0$ for all α and β. This leads to

$$\langle U^2 \rangle = \frac{1}{2} \sum_{\langle i,j \rangle} J_{ij}^{\alpha_1 \beta_1} J_{ij}^{\alpha_2 \beta_2} \left\langle \delta S_i^{\alpha_1} \delta S_i^{\alpha_2} \right\rangle \left\langle \delta S_j^{\beta_1} \delta S_j^{\beta_2} \right\rangle. \quad \text{(C16)}$$

The computational complexity of the method requires the usage of a diagrammatic approach, which we now introduce by considering, for example, the calculation of Eq. (C16).

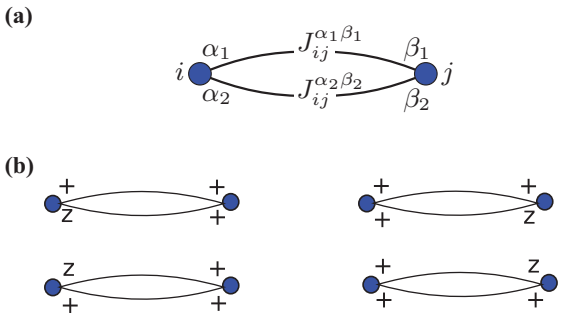

FIG. 6. (Color online) (a) Diagrammatic representation of the term $J_{ij}^{\alpha_1\beta_1} J_{ij}^{\alpha_2\beta_2} \langle \delta S_i^{\alpha_1} \delta S_i^{\alpha_2} \rangle \langle \delta S_j^{\beta_1} \delta S_j^{\beta_2} \rangle$ in Eq. (C16). (b) All diagrams corresponding to $\alpha_i, \beta_i = z, +$, $i = 1,2$ with z appearing only once among the greek superscripts. The same number of diagrams are present for the case where $\alpha_i, \beta_i = z, -$. Again z appears only once.

In this equation, for a given i, j, α_t, and β_t with $t = 1,2$, $J_{ij}^{\alpha_1\beta_1} J_{ij}^{\alpha_2\beta_2} \langle \delta S_i^{\alpha_1} \delta S_i^{\alpha_2} \rangle \langle \delta S_j^{\beta_1} \delta S_j^{\beta_2} \rangle$ can be represented by a diagram of the form illustrated in Fig. 6(a). In this figure, the vertex labels match the labels of the lattice sites that the diagrams cover. Each vertex represents an average of the form $\langle \delta S_i^{\alpha_1} \cdots \delta S_i^{\alpha_t} \rangle$, where t is the number of bonds (solid lines) connected to that vertex. In the case of Eq. (C16) as indicated in Fig. 6(a), the averages are $\langle \delta S_i^{\alpha_1} \delta S_i^{\alpha_2} \rangle$ and $\langle \delta S_j^{\beta_1} \delta S_j^{\beta_2} \rangle$. The bonds represent the elements of the coupling matrix, $J_{ij}^{\alpha\beta}$. It is straightforward combinatorics to take into account only the terms that contribute to the degeneracy-lifting factors, $\cos(3\phi)$ or $\cos(6\phi)$. We next proceed to demonstrate this point.

Based on the symmetry analysis of Sec. II A, we note that since $\langle U^2 \rangle$ involves four powers of $\delta S_i^{\alpha_t}$. $\langle U^2 \rangle$ can only contribute degeneracy-lifting terms of the general form $\propto m_z |m_{xy}|^3 \cos(3\phi)$ and where the proportionality factor is generated by the anisotropic couplings $j_{\pm\pm}$ and $j_{z\pm}$ in Eq. (1c). We recall that $j_{\pm\pm}$ and $j_{z\pm}$ each contributes a factor $e^{\pm 2i\phi}$ and $e^{\pm i\phi}$ in the power counting method. The $-i\phi$ and $-2i\phi$ correspond to the presence of δS^- and $(\delta S^-)^2$ in Eq. (C16), respectively, which in turn, implies the presence of $J_{ij}^- \equiv j_{\pm\pm} \gamma_{ij}^*$ or $J_{ij}^{z-} \equiv j_{z\pm} \zeta_{ij}^*$ matrix elements in $J_{ij}^{\alpha_1\beta_1} J_{ij}^{\alpha_2\beta_2} \langle \delta S_i^{\alpha_1} \delta S_i^{\alpha_2} \rangle \langle \delta S_j^{\beta_1} \delta S_j^{\beta_2} \rangle$. So for a given i and j, only the following combination of terms can generate $\cos(3\phi)$:

$$J_{ij}^{++} J_{ij}^{z+} \langle \delta S_i^+ \delta S_i^+ \rangle \left\langle \delta S_j^z \delta S_j^+ \right\rangle + J_{ij}^- J_{ij}^{z-} \langle \delta S_i^- \delta S_i^- \rangle \left\langle \delta S_j^z \delta S_j^- \right\rangle, \quad \text{(C17)}$$

where the first term generates the $e^{3i\phi}$ contribution to $\cos(3\phi)$ while the second term generates $e^{-3i\phi}$. All possible ways of generating the factor $e^{3i\phi}$ are illustrated in Fig. 6(b), which is the same as the number of ways of generating $e^{-3i\phi}$. Ultimately, Eq. (C16) can be rewritten as

$$\langle U^2 \rangle = 2 j_{\pm\pm} j_{z\pm} \left(\langle \delta S^z \delta S^+ \rangle \langle \delta S^+ \delta S^+ \rangle \sum_{ij} \gamma_{ij} \zeta_{ij} + \text{H.c.} \right). \quad \text{(C18)}$$

Based on Eqs. (C11) and (C14) and recalling from Sec. II that $\boldsymbol{m}$ and ϕ do not require site indices in the Γ_5 manifold, we have dropped the site labels of δS's in Eq. (C16) when

writing Eq. (C18). The lattice sum, $\sum_{ij}\gamma_{ij}\zeta_{ij}$, can be carried out using a computer program for different lattice sizes with linear dimension L. Up to sixth order in the β expansion, the lattice sums *per site* for different terms in Eqs. (C5) are independent of L for $L \geqslant 2$. Accordingly, we have

$$\frac{1}{N}\sum_{ij}\gamma_{ij}\zeta_{ij} = -6. \tag{C19}$$

Using Eqs. (C11) and (C14), the averages in Eq. (C18) can be written as

$$\langle \delta S^z \delta S^+\rangle = \tfrac{18}{45} m_z m_+ + \cdots, \tag{C20}$$

$$\langle \delta S^+ \delta S^+\rangle = \tfrac{18}{45} m_+^2 + \cdots, \tag{C21}$$

where to the lowest order of interest in $\boldsymbol{m}$ which, in this case, is the fourth order, we kept $\lambda^\alpha \simeq 3m^\alpha$ and neglect all higher-order terms. Finally, Eq. (C18) gives

$$\begin{aligned}\langle U^2\rangle/N &= (-0.96 m_z m_+^3 + \text{H.c.}) j_{\pm\pm} j_{z\pm} \\ &= -1.92\, j_{\pm\pm} j_{z\pm} m_z |m_{xy}|^3 \cos(3\phi).\end{aligned} \tag{C22}$$

We note that Eq. (C22) contributes to ω in Eq. (6) which, in turn, is necessary to evaluate $\bar{\eta}_6(j_{\pm\pm}, j_{z\pm})$ in Eq. (11). All other terms in Eq. (C5) involving solely powers of U and no T_n terms can be calculated in a similar way. The number of diagrams increases as one considers higher-order terms in the β expansion of Eq. (10). As a result, finding the number and type of nonzero average of the form of Eq. (C8) is most easily done using a computer program. The details of this type of calculations are presented in Appendix C 4. Some of the diagrams that appear at higher order in the β expansion are illustrated in Fig. 7.

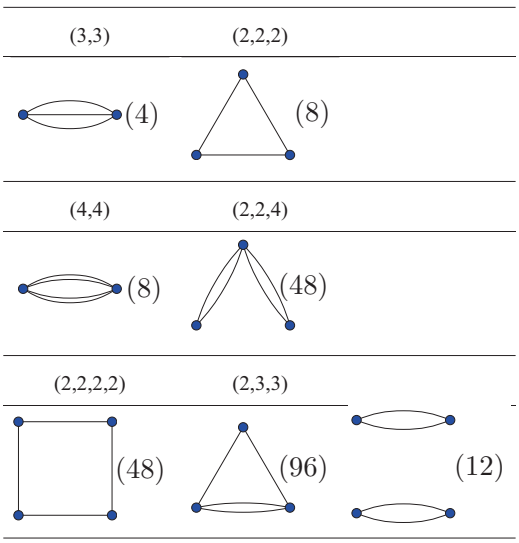

FIG. 7. (Color online) For details, see the text in Appendix C 4. We also note that the contribution of disconnected diagrams (e.g., the diagram at the bottom right corner) in Eq. (C5) adds up to zero.

3. $\langle U^2 T_2\rangle$ Calculation

Due to the presence of T_n in Eq. (C6), in this case $n = 2$, averages that involve T_n need to be carried out slightly differently in comparison with averages containing only powers of U. The difference comes from the presence of the factor $\partial^n \boldsymbol{\lambda}_i/\partial\beta^n$ in Eq. (C6). Considering Eq. (C5a) and the relation $\partial\boldsymbol{\lambda}/\partial\beta|_{\beta=0} = \boldsymbol{h}_i$ [40], we obtain the following relation:

$$\frac{\partial\lambda^\alpha}{\partial\beta} = \frac{\partial\langle H\rangle}{\partial m^\alpha} = \frac{\partial^2(\beta G(\beta))}{\partial m^\alpha \partial\beta}, \tag{C23}$$

From Eq. (C23), one can write

$$\frac{\partial^n\lambda^\alpha}{\partial\beta^n} = \frac{\partial^{n+1}(\beta G(\beta))}{\partial m^\alpha \partial\beta^n}. \tag{C24}$$

Using Eq. (C6), $\langle U^2 T_2\rangle$ can therefore be written as

$$\begin{aligned}\langle U^2 T_2\rangle = \frac{1}{2^2}\sum_{i_1 j_1}\sum_{i_2 j_2}\sum_k J^{\alpha_1\beta_1}_{i_1 j_1} J^{\alpha_2\beta_2}_{i_2 j_2}\frac{\partial^2\lambda_k^{\alpha_3}}{\partial\beta^2} \\ \times\left\langle \delta S^{\alpha_1}_{i_1}\delta S^{\beta_1}_{j_1}\delta S^{\alpha_2}_{i_2}\delta S^{\beta_2}_{j_2}\delta S^{\alpha_3}_k\right\rangle.\end{aligned} \tag{C25}$$

Using Eq. (C24), we have

$$\frac{\partial^2\lambda_k^{\alpha_3}}{\partial\beta^2} = \frac{\partial^3(\beta G(\beta))}{\partial m^\alpha\partial\beta^2} = -\frac{\partial\langle U^2\rangle}{\partial m^{\alpha_3}}. \tag{C26}$$

The term $\langle \delta S^{\alpha_1}_{i_1}\delta S^{\beta_1}_{j_1}\delta S^{\alpha_2}_{i_2}\delta S^{\beta_2}_{j_2}\delta S^{\alpha_3}_k\rangle$ in Eq. (C25) can be dealt with as described previously in Appendix C 1. The outcome reads

$$\left\langle \delta S^{\alpha_1}_{i_1}\delta S^{\beta_1}_{j_1}\delta S^{\alpha_2}_{i_2}\delta S^{\beta_2}_{j_2}\delta S^{\alpha_3}_k\right\rangle = 4\left\langle \delta S^{\alpha_1}_{i_1}\delta S^{\alpha_2}_{i_1}\right\rangle\left\langle \delta S^{\alpha_3}_k\delta S^{\beta_1}_k\delta S^{\beta_2}_k\right\rangle, \tag{C27}$$

where the factor of 4 comes from the number of different ways of pairing site indices yielding nonvanishing results. On the other hand,

$$\langle U^2\rangle = \frac{1}{2}\sum_{ij} J^{\alpha_1\beta_1}_{ij} J^{\alpha_2\beta_2}_{ij}\left\langle \delta S^{\alpha_1}_i\delta S^{\alpha_2}_i\right\rangle\left\langle \delta S^{\beta_1}_j\delta S^{\beta_2}_j\right\rangle, \tag{C28}$$

and, in turn,

$$\frac{\partial\langle U^2\rangle}{\partial m^{\alpha_3}_k} = \frac{\partial\lambda_k^{\alpha_3}}{\partial m_k^{\alpha_3}}\sum_{ij} J^{\alpha_1\beta_1}_{ij} J^{\alpha_2\beta_2}_{ij}\frac{\partial\left\langle \delta S^{\alpha_1}_i\delta S^{\alpha_2}_i\right\rangle}{\partial\lambda_k^{\alpha_3}}\left\langle \delta S^{\beta_1}_j\delta S^{\beta_2}_j\right\rangle, \tag{C29}$$

where $\frac{\partial\lambda_k^{\alpha_3}}{\partial m_k^{\alpha_3}} \simeq 3$. Here, we ignored higher-order terms which do not contribute to the degeneracy lifting terms of fourth or sixth order in components of $\boldsymbol{m}$ in Eq. (C25). The $\frac{\partial\langle \delta S^{\alpha_1}_i\delta S^{\alpha_2}_i\rangle}{\partial\lambda_k^{\alpha_3}}$ expression can be calculated using Eq. (C12). Substituting Eqs. (C27) and (C29) in Eq. (C25), we obtain the final expression which can be represented by a "fused" diagram shown in Fig. 8. This diagram has a new type of vertex represented with a red square. This vertex is labeled with only one site index and its mathematical expression is

$$\left\langle \delta S^{\alpha_3}_k\delta S^{\beta_1}_k\delta S^{\beta_2}_k\right\rangle\left\langle \delta S^{\alpha_3}_k\delta S^{\gamma_1}_k\delta S^{\gamma_2}_k\right\rangle, \tag{C30}$$

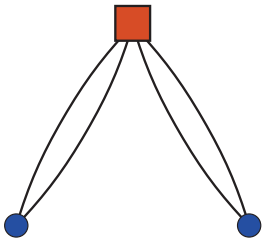

FIG. 8. (Color online) "Fused" diagram corresponding to $\langle U^2 T_2\rangle$. The vertex represented by the (red) square represents the following: $\langle \delta S_k^{\alpha_3} \delta S_k^{\beta_1} \delta S_k^{\beta_2}\rangle \langle \delta S_k^{\alpha_3} \delta S_k^{\gamma_1} \delta S_k^{\gamma_2}\rangle$.

where again there is a sum over repeated greek superscripts. As a result, the final expression reads

$$\langle U^2 T_2\rangle = -\frac{\partial \lambda_k^{\alpha_3}}{\partial m_k^{\alpha_3}} \sum_{ijk} J_{ik}^{\alpha_1\beta_1} J_{ik}^{\alpha_2\beta_2} J_{jk}^{\alpha_3\beta_3} J_{jk}^{\alpha_4\beta_4} \left\langle \delta S_i^{\alpha_1} \delta S_i^{\alpha_2}\right\rangle \times \left\langle \delta S_k^{\alpha_3} \delta S_k^{\beta_1} \delta S_k^{\beta_2}\right\rangle \left\langle \delta S_k^{\alpha_3} \delta S_k^{\beta_3} \delta S_k^{\beta_4}\right\rangle \left\langle \delta S_j^{\alpha_3} \delta S_j^{\alpha_4}\right\rangle. \tag{C31}$$

From this point on, one can adopt the procedure presented previously for the $\langle U^n\rangle$ terms to obtain the final result. All other averages that contain T_n, e.g., $\langle U^{n_1} T_{m_1} T_{m_2}\rangle$ and $\langle T_{n_1}^{m_1} T_{n_2}^{m_2}\rangle$, where n_i, m_i with $i = 1,2$ are natural numbers, can be calculated following a similar procedure.

4. On diagrams

In this section, we make a few comments about the different diagrams that appear in the E-TAP expansion. First, we focus on diagrams corresponding to $\langle U^n\rangle$ with $n = 2,3,\ldots,$ in Eq. (C5). The diagrams for $n = 3,4$ are illustrated in Fig. 7. In this figure, blue circles represent a given lattice site and the number of lines (bonds) connected to the circles is the number of paired δS's at that lattice site. The degree of the vertices is indicated above each diagram and is written in the form of $(\alpha_1,\ldots,\alpha_m)$ where m is the number of vertices and α_i is the number of bonds connected to vertex i. The number of times that each diagram appears in the process of pairing δS's, referred to as diagram count, is indicated in parentheses to the right of each diagram in Fig. 7. The diagrams are distinguished by the degree of their vertices and their adjacency matrix eigenvalues [52]. The adjacency matrix M is a $m \times m$ matrix with matrix elements M_{ij} $(0 < i,j \leqslant m)$ corresponding to the number of lines connecting the ith vertex to the jth vertex. We enumerate these diagrams using a computer program in which we generate all possible diagrams given a certain number of vertices of a given degree. Then, we remove all diagrams that include any onsite interactions which are forbidden since there is no onsite interaction in the Hamiltonian of Eq. (1). For the remaining diagrams, we build their adjacency matrix which we then diagonalize. M is a symmetric matrix and thus has a set of real eigenvalues which defines a graph equivalence class. Graph with the same adjacency matrix eigenvalues correspond to graphs with the same topology, i.e., they are isomorphic [61]. The number of graphs with a given topology is noted in parentheses to the right of the graph in Fig. 7.

The fifth and sixth order terms of the E-TAP expansion in β, contain, respectively, 9 and 26 types of connected diagrams. We note that the contribution of disconnected diagrams in Eq. (C5) adds up to zero [52].

The so-called fused diagrams appear in terms of the form $\langle U^m T_n\rangle$ and $\langle T_m T_n\rangle$, where $m,n \geqslant 2$ are positive integers. They are constructed by fusing the diagrams similar to the ones in Fig. 7 together. An example of such a fused diagram and the corresponding details of its definition is given in the caption of Fig. 8.

We note that some of the diagrams do not cover lattice sites beyond one tetrahedron, for example, the triangular diagram and the two site diagram in the top row of Fig. 7. Only, diagrams of this type contribute to fluctuations incorporated in the cluster mean-field theory (c-MFT) calculations. However, their effect is incorporated to all orders in β in the c-MFT calculation.

[1] P. M. Chaikin and T. C. Lubensky, *Principles of Condensed Matter Physics* (Cambridge University Press, Cambridge, UK, 1994), Chap. 5.

[2] J. N. Reimers, A. J. Berlinsky, and A.-C. Shi, Phys. Rev. B **43**, 865 (1991).

[3] M. Enjalran and M. J. P. Gingras, Phys. Rev. B **70**, 174426 (2004).

[4] J. Villain, R. Bidaux, J.-P. Carton, and R. Conte, J. Phys. (Paris) **41**, 1263 (1980).

[5] E. F. Shender, Zh. Eksp. Teor. Fiz. **83**, 326 (1982) [JETP **56**, 178 (1982)].

[6] C. L. Henley, Phys. Rev. Lett. **62**, 2056 (1989).

[7] *Fluctuations and Order: The New Synthesis*, edited by M. Millonas (Springer, New York, 1996), Chap. 16.

[8] T. Yildirim, Turk. J. Phys. **23**, 47 (1999).

[9] S. Sachdev, Phys. Rev. B **45**, 12377 (1992).

[10] R. Moessner and J. T. Chalker, Phys. Rev. B **58**, 12049 (1998).

[11] J. T. Chalker, P. C. W. Holdsworth, and E. F. Shender, Phys. Rev. Lett. **68**, 855 (1992).

[12] G.-W. Chern and R. Moessner, Phys. Rev. Lett. **110**, 077201 (2013).

[13] V. S. Maryasin and M. E. Zhitomirsky, Phys. Rev. Lett. **111**, 247201 (2013).

[14] P. A. McClarty, P. Stasiak, and M. J. P. Gingras, Phys. Rev. B **89**, 024425 (2014).

[15] M. E. Zhitomirsky, M. V. Gvozdikova, P. C. W. Holdsworth, and R. Moessner, Phys. Rev. Lett. **109**, 077204 (2012).

[16] L. Savary, K. A. Ross, B. D. Gaulin, J. P. C. Ruff, and L. Balents, Phys. Rev. Lett. **109**, 167201 (2012).

[17] A. W. C. Wong, Z. Hao, and M. J. P. Gingras, Phys. Rev. B **88**, 144402 (2013).

[18] J. Oitmaa, R. R. P. Singh, B. Javanparast, A. G. R. Day, B. V. Bagheri, and M. J. P. Gingras, Phys. Rev. B **88**, 220404 (2013).

[19] T. Buckel, B. Dorner, A. Gukasov, and V. Plakhty, Phys. Lett. A **162**, 357 (1992).

[20] A. G. Gukasov, T. Buckel, B. Dorner, V. P. Plakhty, W. Prandl, E. F. Shender, and O. P. Smirnov, Europhys. Lett. **7**, 83 (1988).

[21] Y. J. Kim, A. Aharony, R. J. Birgeneau, F. C. Chou, O. Entin-Wohlman, R. W. Erwin, M. Greven, A. B. Harris, M. A. Kastner, I. Y. Korenblit, Y. S. Lee, and G. Shirane, Phys. Rev. Lett. **83**, 852 (1999).

[22] J. D. M. Champion, M. J. Harris, P. C. W. Holdsworth, A. S. Wills, G. Balakrishnan, S. T. Bramwell, E. Čižmár, T. Fennell, J. S. Gardner, J. Lago, D. F. McMorrow, M. Orendáč, A. Orendáčová, D. M. Paul, R. I. Smith, M. T. F. Telling, and A. Wildes, Phys. Rev. B **68**, 020401 (2003).

[23] J. D. M. Champion and P. C. W. Holdsworth, J. Phys.: Condens. Matter **16**, S665 (2004).

[24] S. T. Bramwell, M. J. P. Gingras, and J. N. Reimers, J. Appl. Phys. **75**, 5523 (1994).

[25] J. S. Gardner, M. J. P. Gingras, and J. E. Greedan, Rev. Mod. Phys. **82**, 53 (2010).

[26] A. Poole, A. Wills, and E. Lelièvre-Berna, J. Phys.: Condens. Matter **19**, 452201 (2007).

[27] J. P. C. Ruff, J. P. Clancy, A. Bourque, M. A. White, M. Ramazanoglu, J. S. Gardner, Y. Qiu, J. R. D. Copley, M. B. Johnson, H. A. Dabkowska, and B. D. Gaulin, Phys. Rev. Lett. **101**, 147205 (2008).

[28] P. Dalmas de Réotier, A. Yaouanc, Y. Chapuis, S. H. Curnoe, B. Grenier, E. Ressouche, C. Marin, J. Lago, C. Baines, and S. R. Giblin, Phys. Rev. B **86**, 104424 (2012).

[29] K. A. Ross, Y. Qiu, J. R. D. Copley, H. A. Dabkowska, and B. D. Gaulin, Phys. Rev. Lett. **112**, 057201 (2014).

[30] S. Petit, J. Robert, S. Guitteny, P. Bonville, C. Decorse, J. Ollivier, H. Mutka, M. J. P. Gingras, and I. Mirebeau, Phys. Rev. B **90**, 060410 (2014).

[31] H. Yan, O. Benton, L. D. C. Jaubert, and N. Shannon, arXiv:1311.3501 [cond-mat.str-el].

[32] M. E. Zhitomirsky, P. C. W. Holdsworth, and R. Moessner, Phys. Rev. B **89**, 140403 (2014).

[33] G.-W. Chern, arXiv:1008.3038.

[34] B. Canals, M. Elhajal, and C. Lacroix, Phys. Rev. B **78**, 214431 (2008).

[35] B. Javanparast, Z. Hao, M. Enjalran, and M. J. P. Gingras, Phys. Rev. Lett. **114**, 130601 (2015).

[36] G.-W. Chern, R. Moessner, and O. Tchernyshyov, Phys. Rev. B **78**, 144418 (2008).

[37] C. Pinettes, B. Canals, and C. Lacroix, Phys. Rev. B **66**, 024422 (2002).

[38] D. J. Thouless, P. W. Anderson, and R. G. Palmer, Philos. Mag. **35**, 593 (1977).

[39] T. Plefka, J. Phys. A **15**, 1971 (1982).

[40] A. Georges and J. S. Yedidia, J. Phys. A **24**, 2173 (1991).

[41] A. Paramekanti and E. Zhao, Phys. Rev. B **75**, 140507 (2007).

[42] D. Yamamoto, G. Marmorini, and I. Danshita, Phys. Rev. Lett. **112**, 127203 (2014).

[43] P. A. McClarty, S. H. Curnoe, and M. J. P. Gingras, J. Phys.: Conf. Ser. **145**, 012032 (2009).

[44] K. A. Ross, L. Savary, B. D. Gaulin, and L. Balents, Phys. Rev. X **1**, 021002 (2011).

[45] H. R. Molavian, M. J. P. Gingras, and B. Canals, Phys. Rev. Lett. **98**, 157204 (2007).

[46] H. R. Molavian, P. A. McClarty, and M. J. P. Gingras, arXiv:0912.2957 [cond-mat.stat-mech].

[47] J. D. Thompson, P. A. McClarty, H. M. Rønnow, L. P. Regnault, A. Sorge, and M. J. P. Gingras, Phys. Rev. Lett. **106**, 187202 (2011).

[48] L. Savary and L. Balents, Phys. Rev. Lett. **108**, 037202 (2012).

[49] Y.-P. Huang, G. Chen, and M. Hermele, Phys. Rev. Lett. **112**, 167203 (2014).

[50] J. Lou, A. W. Sandvik, and L. Balents, Phys. Rev. Lett. **99**, 207203 (2007).

[51] K. H. Fischer and J. A. Hertz, *Spin Glasses*, Cambridge Studies in Magnetism (Cambridge University Press, Cambridge, UK, 1991).

[52] J. Oitmaa, C. Hamer, and W. Zheng, *Series Expansion Methods for Strongly Interacting Lattice Models* (Cambridge University Press, Cambridge, UK, 2006).

[53] S. E. Palmer and J. T. Chalker, Phys. Rev. B **62**, 488 (2000).

[54] A. W. Sandvik, AIP Conf. Proc. **1297**, 135 (2010).

[55] V. S. Maryasin and M. E. Zhitomirsky, Phys. Rev. B **90**, 094412 (2014).

[56] A. Andreanov and P. A. McClarty, Phys. Rev. B **91**, 064401 (2015).

[57] S. H. Curnoe, Phys. Rev. B **78**, 094418 (2008).

[58] M. R. Roser and L. R. Corruccini, Phys. Rev. Lett. **65**, 1064 (1990).

[59] J. P. Bouchaud and P. G. Zérah, Phys. Rev. B **47**, 9095 (1993).

[60] M. Opper and D. Saad, *Advanced Mean Field Methods: Theory and Practice* (The MIT Press, Cambridge, Massachusetts, USA, 2001), Chap. 2.

[61] R. Diestel, *Graph Theory*, in Graduate Texts in Mathematics (Springer-Verlag, Berlin, Heidelberg, 2010).